

## Volumetric rates of Luminous Red Novae and Intermediate Luminosity Red Transients with the Zwicky Transient Facility

VIRAJ R. KARAMBELKAR,<sup>1</sup> MANSI M. KASLIWAL,<sup>1</sup> NADEJDA BLAGORODNOVA,<sup>2</sup> JESPER SOLLERMAN,<sup>3</sup> ROBERT ALOISI,<sup>4</sup> SHREYA G. ANAND,<sup>1</sup> IGOR ANDREONI,<sup>5,6,7</sup> THOMAS G. BRINK,<sup>8</sup> RACHEL BRUCH,<sup>9</sup> DAVID COOK,<sup>10</sup> KAUSTAV KASHYAP DAS,<sup>1</sup> KISHALAY DE,<sup>11</sup> ANDREW DRAKE,<sup>1</sup> ALEXEI V. FILIPPENKO,<sup>8</sup> CHRISTOFFER FREMLING,<sup>12,13</sup> GEORGE HELOU,<sup>10</sup> ANNA HO,<sup>14</sup> JACOB JENCSON,<sup>15</sup> DAVID JONES,<sup>16,17</sup> RUSS R. LAHER,<sup>18</sup> FRANK J. MASCI,<sup>18</sup> KISHORE C. PATRA,<sup>19</sup> JOSIAH PURDUM,<sup>13</sup> ALEXANDER REEDY,<sup>1</sup> TAWNY SIT,<sup>20</sup> YASHVI SHARMA,<sup>1</sup> ANASTASIOS TZANIDAKIS,<sup>21</sup> STÉFAN J. VAN DER WALT,<sup>22</sup> YUHAN YAO,<sup>1</sup> AND CHAORAN ZHANG<sup>23</sup>

<sup>1</sup>*Cahill Center for Astrophysics, California Institute of Technology, Pasadena, CA 91125, USA*

<sup>2</sup>*Department of Astrophysics/IMAPP, Radboud University, Nijmegen, The Netherlands*

<sup>3</sup>*The Oskar Klein Centre, Department of Astronomy, Stockholm University, AlbaNova, SE-10691 Stockholm, Sweden*

<sup>4</sup>*Department of Astronomy, University of Wisconsin-Madison, 475 North Charter Street, Madison, WI 53706, USA*

<sup>5</sup>*Joint Space-Science Institute, University of Maryland, College Park, MD 20742, USA*

<sup>6</sup>*Department of Astronomy, University of Maryland, College Park, MD 20742, USA*

<sup>7</sup>*Astrophysics Science Division, NASA Goddard Space Flight Center, Mail Code 661, Greenbelt, MD 20771, USA*

<sup>8</sup>*Department of Astronomy, University of California, Berkeley, CA 94720-3411, USA*

<sup>9</sup>*Department of Particle Physics and Astrophysics, Weizmann Institute of Science, 234 Herzl St, 76100 Rehovot, Israel*

<sup>10</sup>*IPAC, California Institute of Technology, 1200 E. California Blvd, Pasadena, CA 91125, USA*

<sup>11</sup>*MIT-Kavli Institute for Astrophysics and Space Research, 77 Massachusetts Ave., Cambridge, MA 02139, USA*

<sup>12</sup>*Cahill Center for Astrophysics, California Institute of Technology, Pasadena, CA 91125, USA*

<sup>13</sup>*Caltech Optical Observatories, California Institute of Technology, Pasadena, CA 91125, USA*

<sup>14</sup>*Department of Astronomy, Cornell University, Ithaca, NY 14853, USA*

<sup>15</sup>*Department of Physics and Astronomy, Johns Hopkins University, 3400 North Charles Street, Baltimore, MD 21218, USA*

<sup>16</sup>*Instituto de Astrofísica de Canarias, E-38205 La Laguna, Tenerife, Spain*

<sup>17</sup>*Departamento de Astrofísica, Universidad de La Laguna, E-38206 La Laguna, Tenerife, Spain*

<sup>18</sup>*IPAC, California Institute of Technology, 1200 E. California Blvd, Pasadena, CA 91125, USA*

<sup>19</sup>*Nagaraj-Noll-Otellini Graduate Fellow, Department of Astronomy, University of California, Berkeley, CA 94720-3411, USA*

<sup>20</sup>*Department of Astronomy, The Ohio State University, 140 West 18th Avenue, Columbus, OH 43210, USA*

<sup>21</sup>*Department of Astronomy, University of Washington, Seattle, WA 98195, USA*

<sup>22</sup>*Berkeley Institute for Data Science, University of California, Berkeley*

<sup>23</sup>*Center for Gravitation, Cosmology, and Astrophysics, Department of Physics, University of Wisconsin, Milwaukee, WI 53201, USA*

### ABSTRACT

Luminous red novae (LRNe) are transients characterized by low luminosities and expansion velocities, and are associated with mergers or common envelope ejections in stellar binaries. Intermediate-luminosity red transients (ILRTs) are an observationally similar class with unknown origins, but generally believed to either be electron capture supernovae (ECSN) in super-AGB stars, or outbursts in dusty luminous blue variables (LBVs). In this paper, we present a systematic sample of 8 LRNe and 8 ILRTs detected as part of the Census of the Local Universe (CLU) experiment on the Zwicky Transient Facility (ZTF). The CLU experiment spectroscopically classifies ZTF transients associated with nearby ( $< 150$  Mpc) galaxies, achieving 80% completeness for  $m_r < 20$  mag. Using the ZTF-CLU sample, we derive the first systematic LRNe volumetric-rate of  $7.8_{-3.7}^{+6.5} \times 10^{-5} \text{ Mpc}^{-3} \text{ yr}^{-1}$  in the luminosity range  $-16 \leq M_r \leq -11$  mag. We find that in this luminosity range, the LRN rate scales as  $dN/dL \propto L^{-2.5 \pm 0.3}$  – significantly steeper than the previously derived scaling of  $L^{-1.4 \pm 0.3}$  for lower luminosity LRNe ( $M_V \geq -10$ ). The steeper power law for LRNe at high luminosities is consistent with the massive merger rates predicted by binary population synthesis models. We find that the rates of the brightest LRNe ( $M_r \leq -13$  mag) are consistent with a significant fraction of

them being progenitors of double compact objects (DCOs) that merge within a Hubble time. For ILRTs, we derive a volumetric rate of  $2.6_{-1.4}^{+1.8} \times 10^{-6} \text{ Mpc}^{-3} \text{ yr}^{-1}$  for  $M_r \leq -13.5$ , that scales as  $dN/dL \propto L^{-2.5 \pm 0.5}$ . This rate is  $\approx 1 - 5\%$  of the local core-collapse supernova rate, and is consistent with theoretical ECSN rate estimates.

## 1. INTRODUCTION

The advent of time domain surveys in the last decades has led to the discovery of “gap transients” – a new class of explosions that have  $-16 \leq M_V \leq -10$  and occupy the luminosity gap between novae and supernovae (SNe) (Kasliwal et al. 2011; Pastorello & Fraser 2019). This class includes a diverse variety of transients such as faint core-collapse SNe (Yang et al. 2021), Ia-like SNe (Bildsten et al. 2007), low-luminosity Iax SNe (Karambelkar et al. 2021), luminous red novae (LRNe, Kulkarni et al. 2007), intermediate luminosity red transients (ILRTs, Thompson et al. 2009) and outbursts in luminous blue variable (LBV) stars (Smith et al. 2011). Among gap transients, there is a sub-class of hydrogen-rich explosions characterized by low expansion velocities and interaction with surrounding circumstellar material (CSM). This sub-class comprises of LRNe, ILRTs and LBV outbursts.

LRNe are transients associated with the final stages of common envelope evolution (CEE) in a stellar binary system (Ivanova et al. 2013a; Tylenda 2005; Pastorello et al. 2019a). The loss of angular momentum in a binary can initiate CEE that terminates with the inspiral of the binary on dynamical timescales. This can either lead to the merger of the two stars or the ejection of the CE and formation of a stable binary in a tighter orbit. Both cases are accompanied by energetic outbursts that are powered primarily by shocks or recombination in the ejected material (Ivanova et al. 2013a; MacLeod et al. 2017; Pejcha et al. 2017; Matsumoto & Metzger 2022). The association of LRNe with CE-related outbursts was supported by the discovery of V1309Sco – a Galactic LRN with archival photometric data showing a binary with a rapidly decaying orbital period in the years leading to the transient (Tylenda et al. 2011). LRNe thus present an opportunity to probe the poorly understood physics of CEE, see Ivanova et al. (2013b). This is of particular importance because CEE is a crucial phase in the formation of double compact objects (DCOs, Vigna-Gómez et al. 2020) that merge to radiate gravitational waves, which are being detected regularly by LIGO (The LIGO Scientific Collaboration et al. 2021a).

LRNe generally have low expansion velocities ( $< 1000 \text{ km s}^{-1}$ ), a wide range of luminosities ( $-3 < M_V < -16$ ), long lasting ( $\sim 100$  day) multi-peaked

light curves that redden rapidly due to dust formation (Kamiński & Tylenda 2011; Kamiński et al. 2015). Prior to 2021, only 4 Galactic and 11 extragalactic LRNe were known (Kochanek et al. 2014; Blagorodnova et al. 2021 and references therein). The extragalactic LRNe have  $-9 \leq M_{\text{peak}} \leq -15$ , while the Galactic LRNe in general have much lower luminosities. Progenitor primary stars have been identified for 7 LRNe so far and have revealed interesting correlations between the masses and peak luminosities (Blagorodnova et al. 2021; Pastorello et al. 2019a). Despite these advances, the volumetric rates of LRNe are largely unconstrained. The best estimate of the rate comes from Kochanek et al. (2014), who used 3 Galactic LRNe that had  $-4 < M_V < -10$  discovered over the last 30 years to determine their rate in the Milky Way. They find that very low luminosity events ( $M_{r/V, \text{peak}} \approx -3$  mag) are fairly common ( $\sim 0.5 \text{ yr}^{-1}$ ), but the rate drops as  $\approx L^{-1.4}$  with increasing luminosity. The rate of the more luminous, extragalactic LRNe has not been measured yet; and extrapolations based on the Galactic rate disagree by orders of magnitude with the expectations from population synthesis (Howitt et al. 2020). An accurate measurement of the rate and luminosity function of LRNe is needed to probe several CEE parameters (see Howitt et al. 2020 for examples).

ILRTs are an observationally related class of transients that are also characterized by low expansion velocities and reddening photometric evolution, but have single-peaked lightcurves and a narrower luminosity range ( $-11 < M_V < -15$ ) compared to LRNe (Cai et al. 2021). The origin of ILRTs still remains a mystery. They have been proposed to be electron-capture SNe in super-AGB stars (Botticella et al. 2009; Cai et al. 2021) or outbursts in dusty LBV stars (Smith et al. 2009; Andrews et al. 2021). Both explanations are supported by the peculiar progenitors of ILRTs. The ILRTs SN 2008S, NGC 300 OT, AT 2019abn have been associated with extremely dusty, infrared-(IR) bright progenitors (Botticella et al. 2009; Prieto et al. 2008; Jencson et al. 2019) consistent with super-AGB stars, while the proposed ILRT AT 2019krl was associated with a blue supergiant or LBV progenitor (Andrews et al. 2021). About a dozen ILRTs have been studied extensively in the last decade (see Cai et al. 2021 and references). Similar to LRNe, the volumetric rate has not been reliably measured. Based on two ILRTs

SN 2008S and NGC 300 OT, Thompson et al. (2009) estimate the ILRT rate to be  $\approx 20\%$  of the CCSN rate. Cai et al. (2021) use a sample of 5 ILRTs reported by different surveys over the last decade and estimate a lower limit of  $\approx 8\%$  of the CCSN rate.

Reliable LRNe and ILRTs rate measurements have been hindered by their heterogeneous sample. The existing rate estimates have used transients reported by different surveys, and have not accounted for effects of survey completeness or selection biases (Kochanek et al. 2014; Cai et al. 2021). A systematic sample of LRNe and ILRTs, preferably from a single survey is required to accurately constrain their rate. Such studies are now possible with experiments like the Census of the Local Universe (CLU, De et al. 2020) on the Zwicky Transient Facility (ZTF, Bellm et al. 2019; Graham et al. 2019; Dekany et al. 2020). ZTF is an optical time domain survey with a 47 sq. deg field-of-view that surveys the entire accessible northern sky at a cadence of  $\approx 2 - 3$  days in the  $g$  and  $r$  bands down to a depth of 20.5 mag. The CLU experiment aims to build a spectroscopically complete sample of transients detected by ZTF that are associated with galaxies in the CLU galaxy catalog (Cook et al. 2019) to a depth of  $m_r \approx 20$  mag. The CLU experiment is ideal to detect low luminosity ( $M_r \leq -16$ ) transients like LRNe and ILRTs out to large distances ( $\approx 100$  Mpc), consequently building a large sample of such rare transients.

In this paper, we present a systematic sample of LRNe and ILRTs detected by the ZTF CLU experiment from June 1, 2018 to February 20, 2022. We utilize this sample and the actual observation history of ZTF to derive the rates of LRNe and ILRTs. In Sec. 2.1, we describe the selection criteria used to construct our LRN and ILRT samples. Sec. 2.1 also describes the photometric and spectroscopic properties of LRNe and ILRTs identified in the CLU experiment. Sec. 3 describes our methods to derive the luminosity function and volumetric rates of LRNe and ILRTs. Sec. 4 compares our results to previous measurements and theoretical predictions, and discusses the implications for progenitors of LRNe and ILRTs. We conclude with a summary of our results in Sec. 5.

## 2. SAMPLE SELECTION

### 2.1. Candidate filtering

We focus our search on transients discovered as part of the ZTF CLU experiment (De et al. 2020). Briefly, CLU aims to build a spectroscopically complete sample of transients associated with galaxies in the local universe ( $< 200$  Mpc). The CLU experiment uses alerts generated from all three (public, collaboration and Cal-

tech) components of the ZTF survey (see De et al. 2020 for details). CLU uses the platform `skyportal` to save and coordinate followup of sources (van der Walt et al. 2019). During ZTF Phase I (2018 June 01 – 2020 October 30), the experiment was limited to all transients that 1) were within  $100''$  of known galaxies in the CLU galaxy catalog (Cook et al. 2019), 2) had more than two detections in ZTF- $g$  or  $r$  filters, and 3) were brighter than  $m_r = 20$  mag. Starting 2020 October 30 (ZTF Phase II), the filtering criteria were updated to select transients that were 1) within 100 kpc of CLU galaxies closer than 140 Mpc, 2) brighter than  $m_r = 20.5$  mag, and 3) less luminous than  $M_r = -17$  mag. A total of 3442 transients were saved by the CLU experiment since start of the ZTF survey. The experiment achieved a spectroscopic completeness of 88.5% in ZTF Phase I and 79% in ZTF phase II for sources brighter than 20 mag.

Candidate LRNe and ILRTs were selected from their real-time ZTF alert photometry using the following selection criteria –

- the transient must pass the CLU selection criteria,
- the transient must be less luminous than  $M_r = -16$  mag,
- the transient must have two ZTF alerts (i.e. two  $> 5\sigma$  detections) brighter than 20 mag in either  $g$  or  $r$  bands.

The sample presented in this paper is restricted to events saved before 2022 February 20.

523 transients satisfied the selection criteria listed above. 109 of these were found to lie on top of faint underlying galaxies that are not present in the CLU catalog. These transients were excluded as they are likely supernovae in distant host galaxies. 55 additional candidates were excluded as they were flagged as image processing artifacts on visual inspection of the difference images. 73 candidates were eliminated as they showed small, long-term ( $> 1$  year) variations in brightness without significant colour changes, and were coincident with stars in the Milky Way or nearby galaxies (M31 or M33).

To further filter our candidates, we used follow-up spectroscopic observations (either from our followup campaigns or on TNS). In addition to the CLU experiment, some of our spectra were collected as part of the ZTF Bright Transient Survey (BTS, Fremling et al. 2020; Perley et al. 2020). The BTS classifications are already public, while all CLU classifications will be presented in separate papers focusing on different sub-samples (e.g. De et al. 2020, Tzanidakis et al.

**Table 1.** Properties of the 34 ZTF transients of interest

ZTF Name	AT Name	$M_{\text{abs}}$ at peak	multi-peak/ plateau	Archival (PTF/ATLAS)	Gal type <sup>a</sup>	$H\alpha$ -FWHM <sup>b</sup> ( $\text{km s}^{-1}$ )	[Ca II]	Mol. feats.	Classification
ZTF18acbwfza*	18hso	$-13.82 \pm 0.15$	mp	-/no	SB(r)a pec	500	em?	yes <sup>c</sup>	LRN-gold
ZTF19adakuot	19zhd	$-9.60 \pm 0.15$	pl	no/yes	SA(s)b			yes <sup>c</sup>	LRN-gold
ZTF20aawdwch*	20hat	$-11.43 \pm 0.15$	pl	no/no	SAB(rs)cd	130	no	yes	LRN-gold
ZTF21aancgbm*	21biy	$-13.86 \pm 0.15$	mp	yes/no	SB(s)d.	500	em?	yes	LRN-gold
ZTF21aagppzg*	21blu	$-13.50 \pm 0.15$	mp	no/no	starforming	500	no	yes	LRN-gold
ZTF21acpkzcc*	21aess	$-15.12 \pm 0.15$	mp	-/no	SB(s)m?	500	no	-	LRN-gold
ZTF18abwxrhi*	18gzz	$-14.50 \pm 0.16$	mp	no/no	(R')SB(rs)ab	300	no	no	LRN-silver
ZTF21aaekeqd*	21afy	$-13.95 \pm 0.16$	pl	-/no	starforming	700	no	no	LRN-silver
ZTF18aajgqmr	20ifb	$-15.36 \pm 0.17$	mp	-/no	starforming				LRN-bronze
ZTF20abjgdec	20afdb	$-14.37 \pm 0.16$	mp	-/no	starforming				LRN-bronze
ZTF21aabfwwl	21iy	$-15.72 \pm 0.16$	mp	-/no	starforming				LRN-bronze
ZTF18acdyopn	18hcj	$-14.33 \pm 0.19$	no	-/no	SAdm.	300	em	no	ILRT-gold
ZTF19aadyppr*	19abn	$-14.73 \pm 0.15$	no	yes/no.	Sa	700	em	no	ILRT-gold
ZTF19acoaiub*	19udc	$-14.62 \pm 0.15$	no	-/no	SAB(s)a	1250	em	no	ILRT-gold
ZTF19acdrkbh	19sfo	$-14.62 \pm 0.20$	-	-/no	starforming	600	em	no	ILRT-gold
ZTF19aagqkrq*	19ahd	$-13.72 \pm 0.15$	no	-/no.	SA(s)cd	700	em	no	ILRT-gold
ZTF21aclzxex*	21adlx	$-15.68 \pm 0.16$	no	yes/no	Sb	700	em	no	ILRT-silver
ZTF21abtduah*	21vdr	$< -14.96$	-	no/no	SB(s)d:	1300	no	no	ILRT-silver
ZTF21abfxjld	21prj	$< -14.21$	-	no/no.	starforming	$< 300$	no	no	ILRT-silver
ZTF18acrygkg	18lqq	$< -14.14$	no	-/no	SA(s)bc				ILRT-bronze
ZTF19aavwbxs	19fxy	$-14.44 \pm 0.17$	no	-/no	starforming				ILRT-bronze
ZTF19acpmbvd	19wbg	$-14.66 \pm 0.15$	mp	yes/yes	SAB(r)a	1700			LBV?
ZTF20abwilhb	20swt	$-13.87 \pm 0.16$	no.	no/no	Scd	3300	no	no	LBV/Type II?
ZTF21aagydmn	21bug	$-14.36 \pm 0.15$	no	yes/no	SAd	2600	no	no	LBV?
ZTF21aantupk	21efb	$-14.71 \pm 0.15$	no	-/yes	-				LBV/AGN?
ZTF21aclyyfm	21adlw	$-16.03 \pm 0.15$	no	-/yes	SA(rs)b		no	no	LBV?
ZTF21aaitlhy	21afm	$-15.44 \pm 0.15$	mp	yes/yes	SBb				LBV?
ZTF18aawoeho	21ahuh	$-15.51 \pm 0.15$	no	no/no	starburst				?
ZTF20ablmyzj	20afdc	$-15.95 \pm 0.30$	no	-/no	S				?
ZTF20acfxnmv	20afdd	$-14.67 \pm 0.15$	-	-/no	SB(s)cd				?
ZTF20acivtfy	20afde	$-13.72 \pm 0.16$	-	-/no	starforming				?
ZTF21aapngrj	21gcg	$-12.75 \pm 0.15$	no	-/no					?
ZTF21aakbdzz	21czz	$-14.83 \pm 0.10$	no	-/no	S				?
ZTF21aamwyxf	21dtz	$-15.98 \pm 0.15$	no	no/no	E				?

- or unfilled entries indicate instances for which data is not available.

\* : Events used for rate calculation, in Sec. 3; *a* : Galaxy morphologies are taken from NED; *b* : Where multiple spectra are available, the maximum FWHM is reported; *c* : The molecular features are visible in spectra from the literature (see Sec. 2.2.2).

in prep., Sit et al. submitted). Of the CLU transients that pass our criteria, seven sources were spectroscopically classified as active galactic nuclei (AGN), 65 as hydrogen-poor SNe (Ia, Iax, Ca-rich, Ib and Ic SNe), 11 as classical novae, 128 as Type II SNe – based on broad ( $v \geq 5000 \text{ km s}^{-1}$ ) H emission lines. 2 additional candidates were studied low-luminosity Type II SNe (Reguitti et al. 2021; Yang et al. 2021) showing low velocity hy-

drogen lines. We were now left with 73 sources that did not match any of the above categories.

We ran forced point-spread function (PSF) photometry at the location of these 73 sources on all ZTF difference images (Masci et al. 2019). This provides more accurate photometry than the real-time ZTF alerts, and also enables the recovery of sub-threshold ( $> 3\sigma$ ) detections. From this set, 14 candidates were ruled out

as their forced photometry revealed them to have absolute magnitudes brighter than  $-16$  mag. 18 additional sources were ruled out because their forced photometry lightcurves revealed slow, small amplitude long term ( $> 500$  day) variations. These slowly varying sources are likely foreground variable stars, but some could also be long duration giant outbursts in LBV stars such as  $\eta$ -Car or UGC 2773-OT (Humphreys et al. 1999; Smith et al. 2016). One additional source at redshift  $z=0.002$  showed fast erratic variations in ZTF data. Finally, five sources had  $M_r \geq -10$  and fast fading lightcurves ( $< 10$  d), suggesting that they are classical novae. Of the remaining, one source showed a declining lightcurve with  $g-r < 0$  mag, similar to late-time SN lightcurves, unlike LRNe or ILRTs. The remaining 34 sources are promising LRNe and ILRT candidates, and are listed in Table 1.

## 2.2. Classification

The shortlist of 34 transients in Table 1 consists of LRNe, ILRTs, LBV outbursts and possibly some supernovae observed at late phases. Here, we discuss the classifications of these transients using their ZTF lightcurves, spectroscopic data and archival photometry.

LRNe typically show multi-peaked lightcurves (Pejcha et al. 2017; Matsumoto & Metzger 2022) which allows to photometrically differentiate them from ILRTs (Cai et al. 2021). Table 1 indicates the transients that show multiple peaks in their ZTF lightcurves.

Searching for previous outbursts in archival data can help distinguish LBV eruptions from LRNe/ILRTs, as LBV outbursts can be recurring. While LRNe are also known to show precursor emission in the years leading up to the merger, the precursors usually have much lower luminosities than the actual merger. The detection of historic outbursts comparable in brightness to the latest outburst is thus suggestive of an LBV eruption. We checked for historical activity at the locations of these sources using data from the ATLAS (Tonry et al. 2018; Smith et al. 2020, depth  $\approx 19.5$  mag, dating back to  $\sim 2014$ ) and PTF (Law et al. 2009; Rau et al. 2009, depth  $\approx 21.5$  mag, dating back to  $\sim 2009$ ) surveys. All 34 sources have ATLAS data while 15 have PTF data. Table 1 indicates which transients were detected in the archival ATLAS or PTF data. The full forced photometry lightcurves will be available online (see Sec. 7)

Spectroscopic data is available for 19 of the 34 transients. 11 of these sources only have medium resolution optical spectra, while the remaining 8 also have medium resolution NIR spectra. The optical spectra were taken with the Low-Resolution Imaging Spectrograph (LRIS, Oke et al. 1995,  $R \approx 750$ ) on the Keck I

Telescope, the Double Beam Spectrograph (DBSP, Oke & Gunn 1982,  $R \approx 1000$ ) on the 200-inch Hale telescope (P200) on Mount Palomar, the Alhambra Faint Object Spectrograph and Camera (ALFOSC,  $R \approx 360$ ) on the 2.56m Nordic Optical Telescope (NOT), the Kast Double Spectrograph on the Shane 3-m telescope at the Lick Observatory ( $R \approx 1000$ ) and the Spectrograph for Rapid Acquisition of Transients (SPRAT,  $R \approx 350$ ) on the Liverpool Telescope. For ZTF21acpkzcc, we obtained a high resolution ( $R \approx 15000$ ) spectrum with the South African Large Telescope High Resolution Spectrograph (HRS, Bramall et al. 2010). The NIR spectra were taken with the Near-Infrared Echelle Spectrograph (NIRES, Wilson et al. 2004,  $R \approx 2700$ ) on the Keck II telescope and the Triplespec spectrograph (Herter et al. 2008,  $R \approx 2500$ ) on P200. The log of the spectroscopic observations is listed in Table 2. In addition to these, we also obtained several low-resolution ( $R \approx 100$ ) spectra of these transients with the Spectral Energy Distribution Machine (SEDM; Blagorodnova et al. 2018; Rigault et al. 2019; Kim et al. 2022) spectrograph on the 60-inch telescope at Palomar Observatory. These spectra are not discussed here as their resolutions are too low for a useful analysis. All our spectra (including the low-resolution ones) will be made available online (Sec. 7).

LRNe, ILRTs and LBV outbursts can have similar spectroscopic properties especially at early times. However, some LBV eruptions have expansion velocities exceeding  $\approx 2000$  km  $s^{-1}$ , while LRNe and ILRTs have lower expansion velocities (typically  $\sim 1000$  km  $s^{-1}$ ). The FWHM velocities of the  $H\alpha$  emission line in the transients with spectroscopic coverage are listed in Table 1. For transients with multiple spectra, the maximum velocity is listed. Early time spectra of both LRNe and ILRTs are characterized by narrow  $H\alpha$  ( $v_{\text{FWHM}} \leq 1000$  km  $s^{-1}$ ) emission. [Ca II] emission was thought to be a defining feature of ILRTs, however it was recently discovered that some LRNe can show [Ca II] emission (Cai et al. 2019), while some ILRTs do not show [Ca II] at certain phases (Andrews et al. 2021). Late-time spectroscopic observations can help confidently distinguish between LRNe and ILRTs. In LRNe,  $H\alpha$  emission grows narrower and weaker with time since peak, and eventually reemerges. Late-time spectra of LRNe also exhibit molecular absorption features. On the contrary, ILRTs show persistent narrow H emission throughout their evolution. Their late time spectra do not show molecular features, but have strong  $H\alpha$  and Ca II emission lines.

Provided that not all of our sources have late-time spectroscopic coverage, we use the available spectra (from literature wherever necessary) together with the lightcurves to create a classification scheme for these

**Table 2.** Observation log of spectra presented in this paper

Name	Tel./ Inst.	Date	Resolution	Name	Tel./ Inst.	Date	Resolution
ZTF18abwxrhi	P200/DBSP	2018-09-18	1500	ZTF21aancgbm	Keck/NIRES	2021-04-18	1000
ZTF18abwxrhi	P200/DBSP	2018-10-10	1000	ZTF21aagppzg	Keck/NIRES	2021-04-18	1000
ZTF18acbwfza	Gemini/GMOS	2018-11-02	2000	ZTF21aaekeqd	Keck/LRIS	2021-05-09	750
ZTF18acbwfza	P200/DBSP	2018-11-02	1000	ZTF21abfxjld	Keck/LRIS	2021-07-06	750
ZTF18acbwfza	Keck/LRIS	2018-11-10	750	ZTF21abfxjld	Keck/LRIS	2021-08-14	750
ZTF18acdyopn	Keck/LRIS	2018-11-10	750	ZTF21abfxjld	Keck/NIRES	2021-09-25	1000
ZTF19aadyppr	P200/DBSP	2019-01-26	1000	ZTF21abtduah	P200/DBSP	2021-11-06	1000
ZTF19aagqkrq	NOT/ALFOSC	2019-02-11	350	ZTF21aclyyf	P200/DBSP	2021-11-06	1000
ZTF19aagqkrq	P200/DBSP	2019-02-12	1000	ZTF21aclzzex	Shane/KAST	2021-11-12	1000
ZTF19aadyppr	NOT/ALFOSC	2019-02-23	350	ZTF21acpkzcc	Keck/NIRES	2021-11-17	1000
ZTF19aadyppr	Keck/LRIS	2019-03-07	750	ZTF21acpkzcc	SALT/HRS	2021-11-29	15000
ZTF19aadyppr	P200/DBSP	2019-03-16	1000	ZTF21acpkzcc	P200/DBSP	2021-12-01	1000
ZTF19aadyppr	P200/DBSP	2019-04-13	1000	ZTF21abtduah	P200/DBSP	2021-12-01	1000
ZTF19aadyppr	P200/DBSP	2019-05-13	1000	ZTF21aclzzex	P200/DBSP	2021-12-01	1000
ZTF19acdrkbh	Keck/LRIS	2019-10-27	750	ZTF21aagppzg	P200/TSpec	2021-12-12	1000
ZTF19acoaiub	P200/DBSP	2019-11-05	1000	ZTF21acpkzcc	P200/DBSP	2022-01-12	1000
ZTF19acoaiub	Keck/NIRES	2019-12-04	1000	ZTF21acpkzcc	P200/TSpec	2022-01-20	1000
ZTF19acpmbvd	LT/SPRAT	2019-12-23	350	ZTF21aclzzex	Keck/LRIS	2022-01-26	750
ZTF20aawdwch	NOT/ALFOSC	2020-05-15	300	ZTF21aclyyf	P200/DBSP	2022-02-02	1000
ZTF20abwilhb	Keck/LRIS	2020-10-20	750	ZTF21aancgbm	Keck/LRIS	2022-02-03	750
ZTF21aagppzg	P200/DBSP	2021-02-08	1000	ZTF21acpkzcc	Keck/LRIS	2022-02-03	750
ZTF21aaekeqd	Keck/LRIS	2021-02-17	750	ZTF21abtduah	Keck/LRIS	2022-02-03	750
ZTF21aagppzg	P200/DBSP	2021-02-20	1000	ZTF21aclzzex	Keck/LRIS	2022-03-01	750
ZTF21aagydmn	P200/DBSP	2021-02-20	1000	ZTF21abtduah	Keck/LRIS	2022-03-03	750
ZTF21aagppzg	LT/SPRAT	2021-03-19	350	ZTF21aclzzex	Keck/LRIS	2022-03-03	750
ZTF21aancgbm	P200/DBSP	2021-04-09	1000	ZTF21aagppzg	Keck/NIRES	2022-03-16	1000
ZTF21aagppzg	P200/DBSP	2021-04-09	1000	ZTF21aancgbm	Keck/NIRES	2022-03-17	1000
ZTF21aaekeqd	Keck/LRIS	2021-04-14	750	ZTF21aclzzex	Keck/NIRES	2022-03-17	1000
ZTF21aaekeqd	Keck/NIRES	2021-04-18	1000	ZTF21aclzzex	Keck/NIRES	2022-04-15	1000

transients. We classify the 34 transients into eight categories – Possible LBV outbursts, LRN-gold, LRN-silver, LRN-bronze, ILRT-gold, ILRT-silver, ILRT-bronze, and Ambiguous. We describe these categories in detail below. Briefly, for LRNe and ILRTs, the gold sample comprises transients that we can confidently classify in either category, the silver sample comprises transients that have photometry and spectra indicative to their class, but lack smoking gun signatures associated with the class, and the bronze category comprises transients that have photometric evolution similar to their class, but do not have any spectroscopic data. The “Ambiguous” category consists of 7 sources that have poor quality data, i.e. no spectra *and* low-quality sparse photometric coverage owing to bad weather or solar conjunction of the transient, rendering us unable to place them in any of the other categories. Table 1 lists the classification

of these sources based on this scheme. We describe the sources in each category below.

### 2.2.1. Possible LBV eruptions

This category includes sources that show broad ( $v_{\text{FWHM}} \geq 2000 \text{ km s}^{-1}$ )  $\text{H}\alpha$  emission in their spectra, *or* have historic outbursts in archival data. A total of 6 transients in our shortlist satisfy these criteria. Two of these – ZTF 21aagydmn and ZTF 20abwilhb show broad  $\text{H}\alpha$  emission with FWHM velocities of 2600 and 3300  $\text{km s}^{-1}$  and are likely LBV outbursts. The ATLAS and PTF data classifies four additional sources as potential LBVs – ZTF 19acpmbvd, ZTF 21aantupk, ZTF 21aclyyf and ZTF 21aaitlhy. We describe these sources in the Appendix A.

### 2.2.2. LRN-gold

This category includes six spectroscopically confirmed LRNe detected in ZTF data in the last three

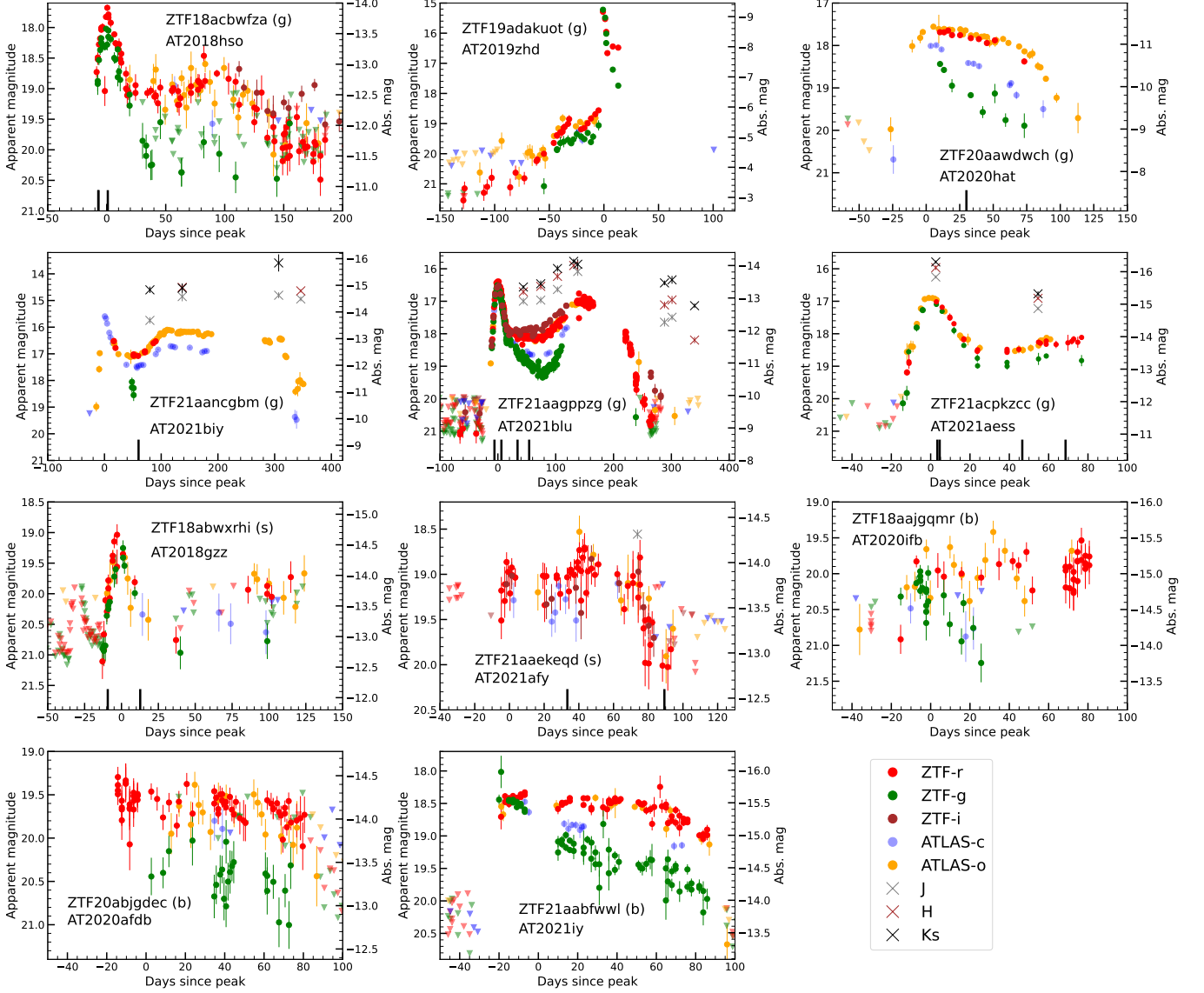


**Figure 1.** Forced photometry lightcurves of the 11 LRNe in our sample. The transients in gold, silver and bronze samples are marked in parantheses with g, s and b respectively. The ZTF-g, ZTF-r, ZTF-i, ATLAS-c and ATLAS-o band datapoints are plotted as green, red, brown, blue and orange points respectively. The J, H and Ks band magnitudes are plotted as gray, brown and black crosses respectively. Downward pointing triangles indicate  $5\text{-}\sigma$  upper limits. The days are in observer frame. The lightcurves have been corrected for extinction using the values listed in Table 3. Solid black vertical lines indicate epochs at which the spectra were obtained.

years. Three of these have been studied in detail previously – ZTF 18acbwfza (AT 2018hso, Cai et al. 2019), ZTF 19adakuot (AT 2019zhd, Pastorello et al. 2021a) and ZTF 20aawdwch (AT 2020hat, Pastorello et al. 2021b). Three other transients – ZTF 21aacgbm (AT 2021biy, Cai et al. 2022), ZTF 21aagppzg (AT 2021blu, Pastorello et al. 2022) and ZTF 21acpkzcc (AT 2021aess, Davis et al. 2021) were identified as possible LRNe in 2021. We initiated optical and NIR photometric and spectroscopic followup campaign for these objects, which confirmed their nature as LRNe.

Our lightcurves of these transients are shown in Fig. 1. For all our calculations, we use host galaxy redshifts corrected for local velocity flows from the NASA Extragalactic Database (NED), and assume  $H_0 = 73 \text{ km s}^{-1} \text{ Mpc}^{-1}$ . We use Milky Way line-of-sight extinction values from Schlafly et al. (2012). We calculate the host galaxy extinctions for LRNe using Na ID equivalent widths in their early time spectra (see discussion of individual objects below). We calculate the peak magnitudes and epoch of maximum brightness by fitting polynomials to the near-peak lightcurve. We

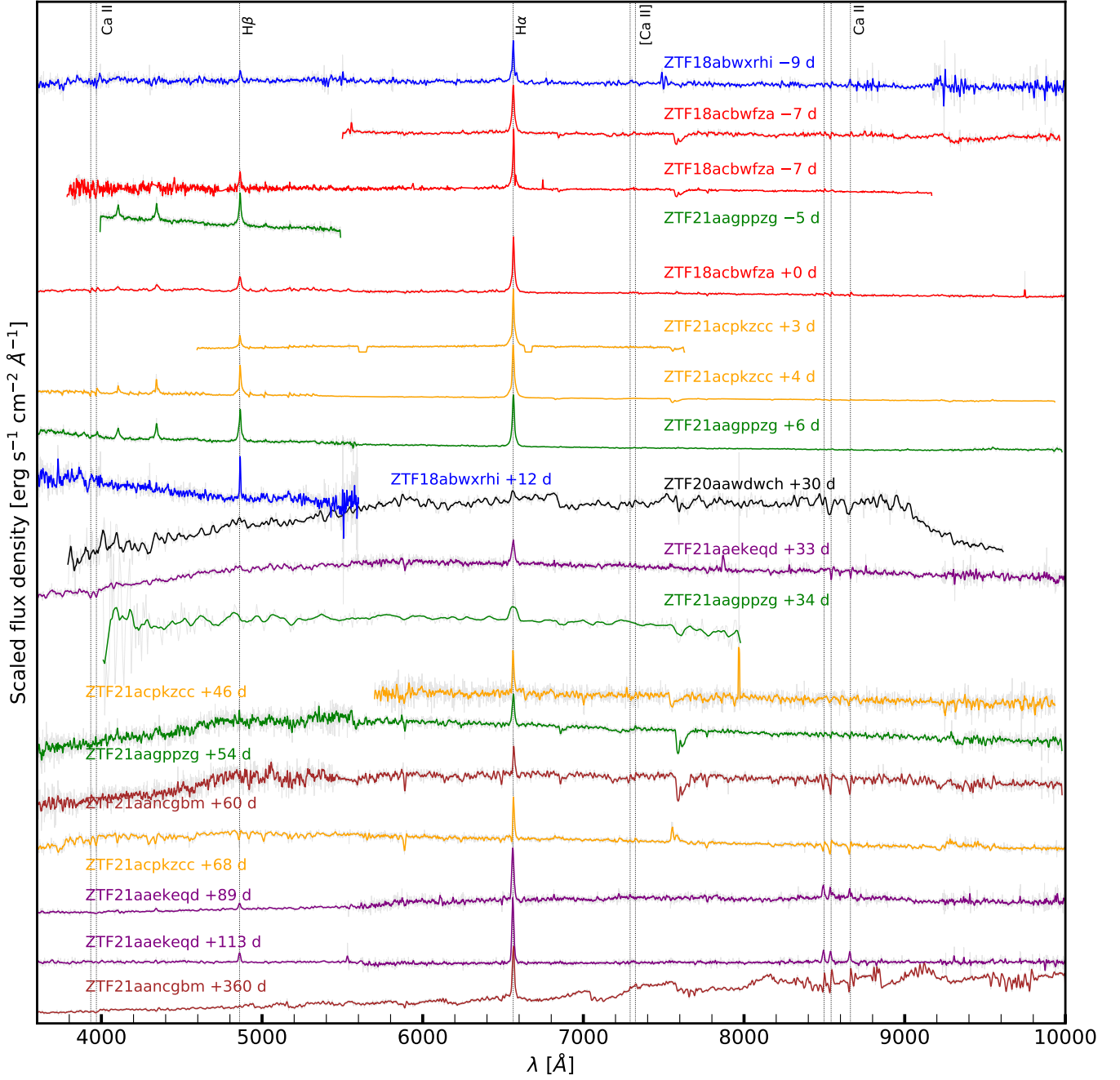


**Figure 2.** Optical spectra for LRNe presented in this paper.

calculate the pseudo-bolometric lightcurves by fitting blackbodies to the available optical data. The derived photometric properties and the adopted distances and extinctions for the LRNe in our sample are listed in Table 3.

Our spectra of these transients are shown in Fig. 2 and 3. We analyze the optical spectra and derive the hydrogen Balmer line velocities by fitting lorentzian profiles (which are better fits than gaussian profiles). We also measure the Balmer decrement ( $\beta$ ) as the ratio of  $H\alpha$

to  $H\beta$  line fluxes in the spectra where both lines are detected. The spectroscopic properties are listed in Table 4. We now briefly describe individual members of our sample.

**1. ZTF 18acbwfza (AT 2018hso)** is located in the star-forming galaxy NGC 3729. Our earliest spectrum (7 days before peak) shows Na ID absorption with an equivalent width of  $1.5 \pm 0.4 \text{ \AA}$ . Assuming the source of this absorption is dust in the interstellar medium and the correlation from Turatto et al. (2003) we de-



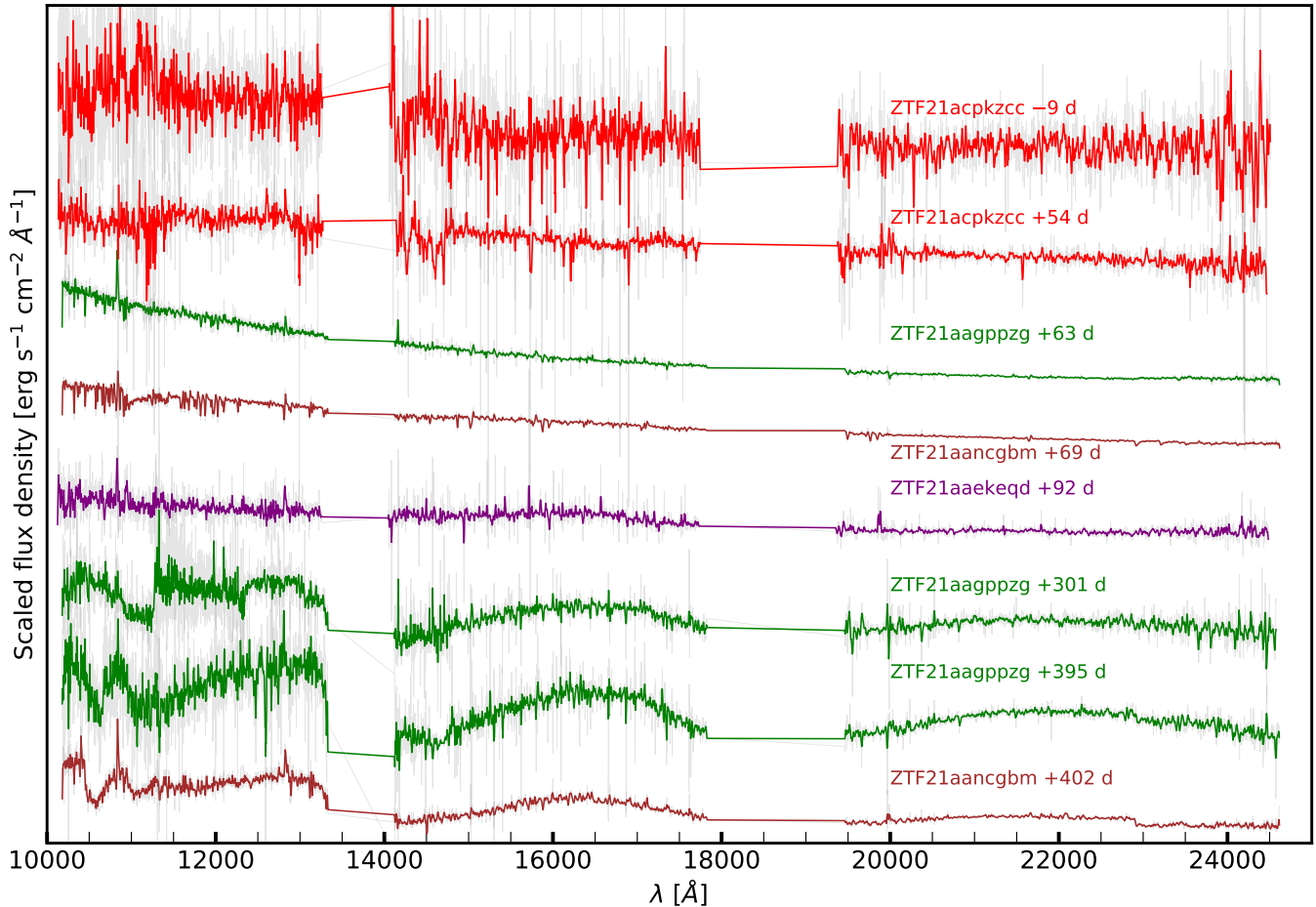


**Figure 3.** NIR spectra for LRNe presented in this paper.

rive  $E(B - V)_{\text{host}} = 0.23 \pm 0.06$  mag. This is consistent with the value used by Cai et al. (2019). The lightcurve is characteristic of LRNe, with an early blue peak lasting for  $\approx 20$  days, followed by a prolonged plateau where the transient evolves rapidly to redder colors. We note that the transient shows signs of evolving back to bluer colors at late times, when the  $r$ -band lightcurve is declining but the  $g$ -band lightcurve has plateaued. However, we caution that the  $g$ -band detections at this phase from ZTF have low significance ( $3\sigma$ ). Our spectra sample only the first blue peak, and show strong Balmer emission lines with  $v_{\text{FWHM}} \approx 500 \text{ km s}^{-1}$ . These spectra also show narrow Ca II NIR triplet lines with a P-cygni profile. The absorption of the P-cygni profile extends to a maximum velocity  $v_m \approx 400 - 500 \text{ km s}^{-1}$ . Cai et al. (2019) report weak [Ca II] in this transient. We find marginal evidence for [Ca II] emission in only one of our spectra, taken 1 day post peak. Late-time spectra from Cai et al. (2019) show strong molecular absorption features.

**2. ZTF 19adakuot (AT 2019zhd)** is located in M31. Following Pastorello et al. (2021a), we assume that the total extinction is dominated by the Milky Way. The

transient has the lowest luminosity in our sample (peaking at  $M_r \approx -9.5$  mag). We do not have any spectroscopic data for this transient, but late-time spectra presented in Pastorello et al. (2021a) show molecular absorption features.

As noted in Pastorello et al. (2021a), this transient shows precursor activity for a few months leading up to the explosion. In these months, the field of ZTF 19adakuot was imaged with the ZTF camera several times per night. We stack the ZTF forced photometry from images taken on the same night, and recover several additional detections than the ones reported in Pastorello et al. (2021a), which are plotted in Fig. 4. We further bin the photometry in bins of ten days to increase the significance of the detections. The ZTF detections date back to 160 days before the  $r$ -band peak, when the transient was first detected at  $m_r \approx 22.7 \pm 0.3$  mag. The binned ZTF lightcurve shows that the transient went through a gradual, bumpy brightening phase for  $\approx 160$  days before the main explosion. Three bumps can be identified in the  $r$ -band lightcurve, each with a duration of  $\approx 50$  days. During each of these bumps, the

transient brightens by an increasing amount ( $\approx 0.5$ , 1 and 2.5 mag respectively) before plateauing or declining by a modest amount ( $\approx 0.5$  mag) at the end of each bump. After the third bump, the transient brightens gradually by  $\approx 1$  mag for 25 days before brightening rapidly by 4 mag as it transitions into the main explosion. This bumpy rise is reminiscent of the pre-outburst evolution of M31-LRN-2015 (Blagorodnova et al. 2020), V838 Mon (Munari et al. 2002; Tylenda 2005) and AT 2020hat (Pastorello et al. 2019b).

At the end of the first bump (MJD 58759), fitting a single blackbody to the  $g$  and  $r$ -band detections suggests a source with  $T_{\text{eff}} = 6600_{-1600}^{+2400}$  K, a radius  $R = 17_{-7}^{+14} R_{\odot}$  and a luminosity of  $5.5_{-0.7}^{+1.3} \times 10^2 L_{\odot}$ . This photosphere is most likely formed by mass outflowing from the outer Lagrangian (L2) point (for example Pejcha et al. 2017 or MacLeod et al. 2022). On the second bump, the transient is only detected in  $r$  band, with the most constraining  $g$  band upper limit giving  $g - r > 0.8$  mag, suggesting the optically thick photosphere has cooled. This likely continues up to the beginning of the third bump on MJD 58837, where the temperature has cooled down to  $T = 3900_{-700}^{+700}$  K and the photosphere has expanded to  $R = 170_{-70}^{+140} R_{\odot}$  and  $L = 6.1_{-1.7}^{+3.9} \times 10^3 L_{\odot}$ . This would imply a photospheric expansion speed of  $\approx 10 - 30 \text{ km s}^{-1}$ . After this, the temperature increases quickly in the next 12 days on the third bump to  $5700_{-300}^{+300}$  K with  $L = 7.5_{-0.3}^{+0.3} \times 10^3 L_{\odot}$ , and reduced  $R = 90_{-12}^{+12} R_{\odot}$  on MJD 58849, suggesting the temperature increase was accompanied by a drop in opacity. This is followed by a surprisingly sharp decline in the redder ( $r$ ,  $o$ ) bands but a slow brightening in the  $g$ -band. During this decline, the temperature increases to  $6900_{-1000}^{+1100}$  K but the radius drops to  $69_{-16}^{+27} R_{\odot}$  with increased luminosity of  $9.5_{-0.6}^{+0.8} \times 10^3 L_{\odot}$  on MJD 58871. This is followed by an increase in luminosity and photospheric radius accompanied by a slight decrease in temperature, to  $L = 1.7_{-0.1}^{+0.2} \times 10^4 L_{\odot}$  on MJD 58887. In the next five days, the transient brightens rapidly to its peak luminosity of  $\approx 5.2 \times 10^5 L_{\odot}$ .

A full analysis of this complex precursor photometric evolution is outside the scope of this paper. A possible explanation for the abrupt temperature increases in this final phase is shocks due to collisions within the L2-stream, as suggested in Pejcha et al. (2017). The total energy radiated during this  $\approx 40$  day duration is  $\approx 10^{44}$  erg. Assuming an L2 velocity of  $30 \text{ km s}^{-1}$ , the mass required in the L2 stream is  $\geq 10^{-2} M_{\odot}$ .

**3. ZTF20aawdwch (AT 2020hat)** is located in NGC 5068. We follow Pastorello et al. (2021b) and assume that the extinction is dominated by the Milky Way. The ZTF lightcurve samples the post-peak decline, starting at

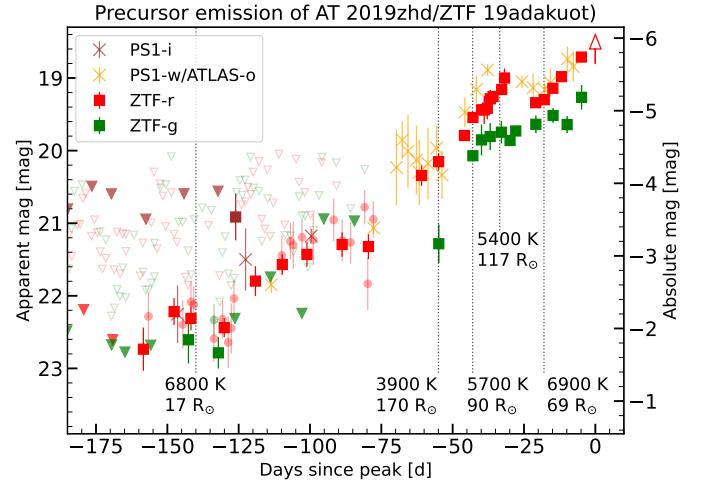


**Figure 4.** Pre-explosion  $g$ ,  $r$  and  $i$ -band detections for ZTF 19adakuot. For phases  $< -75$  days, we bin the ZTF flux measurements taken on the same day to increase the sensitivity. These points are plotted as faint background circles. We further bin these measurements in bins of 10 days to increase their significance. The binned measurements are shown in solid squares. For phases  $> -75$  days, the squares represent ZTF forced photometry from single visits. The triangles denote  $5\text{-}\sigma$  upper limits. The crosses denote measurements reported previously in Pastorello et al. (2021a). At the epochs marked by the dotted vertical lines, we indicate the effective temperatures and photospheric radii to demonstrate the dramatic variations exhibited by the precursor (see text). The initial pre-explosion behaviour is consistent with a photosphere L2-mass loss forming an optically thick photosphere detectable by ZTF at  $\approx -150$  days, which expands and cools up to  $\approx -70$  days. Further collisions in the L2 stream, or accretion onto the companion star can cause sudden increases in temperature over the next 70 days, until the transient brightens rapidly transitioning to the main explosion (marked by the red arrow).

$m_r = 17.90 \pm 0.06$  mag. Our sole spectrum was taken at a phase of 30 days since peak, which shows a reddened continuum, extremely weak  $H\alpha$  emission, some broad but weak molecular absorption features and Ca II NIR triplet absorption lines – characteristic of LRNe on the red plateau phase. Molecular absorption features are clearly detected in late-time spectra presented in Pastorello et al. (2021b).

**4. ZTF 21aancgbm (AT 2021biy, Smith et al. 2021a; Cai et al. 2022)** is located in the galaxy NGC 4631. We do not have spectra at early phases, so we adopt the host extinction derived by Cai et al. (2022) using Na I D absorption. The lightcurve is characteristic of LRNe, with an initial blue peak lasting for  $\approx 50$  days, followed by a rebrightening and a prolonged red plateau of  $\approx 350$  days. The field of ZTF 21aancgbm is not part of the regular 2-day cadence ZTF survey, so the ZTF lightcurve

samples only a small portion of the lightcurve. We combine the ZTF data with ATLAS data, which shows that the lightcurve lasts for more than 400 days, and is the longest duration LRN in our sample.

We obtained *JHKs* NIR imaging with P200/WIRC on several epochs on the plateau, which shows that the transient was significantly brighter in the NIR bands (by  $> 1$  mag) than in the optical (see Fig. 1). The transient shows a late-time bump once it falls off the plateau, likely the result of collision with CSM as noted in Cai et al. (2022). Our spectroscopic coverage comprises two optical spectra at +60 and +360 days since peak, and two NIR spectra at +69 and +402 days since peak. The +60 day spectrum shows a reddened continuum with weak, unresolved H $\alpha$  emission ( $v_{\text{FWHM}} \approx 350 \text{ km s}^{-1}$ ) and Ca II NIR triplet with P-cygni line profiles (with  $v_m \approx 400 \text{ km s}^{-1}$ ). We also detect weak [Ca II] lines with P-cygni line profiles. The +69 d NIR spectrum shows several metallic absorption lines, as well as the CO absorption bandhead. The very late-time optical spectrum at +360 days shows a highly reddened continuum with several strong molecular absorption features of TiO and VO, which confirms the classification as a LRN. This spectrum also shows strong, narrow H $\alpha$  emission (with increased  $v_{\text{FWHM}} \approx 500 \text{ km s}^{-1}$ ) and Ca II NIR lines with P-cygni profiles ( $v_m \approx 600 \text{ km s}^{-1}$ ).

The lightcurve shape and long duration of ZTF 21aancgbm make it an interesting member of the LRN family. The 200 day long plateau resembles that seen in SNe IIP, and it is tempting to posit that it is powered by hydrogen recombination. Matsumoto & Metzger (2022) provide scaling relations between the plateau luminosity ( $L_{\text{pl}}$ ), duration ( $t_{\text{pl}}$ ) and ejected mass ( $M_{\text{ej}}$ ) for a recombination-powered LRN plateau, given by

$$M_{\text{ej}} \approx 1.6 M_{\odot} \times f_{\text{ad},0.3}^{-1} \times \left(\frac{t_{\text{pl}}}{100\text{d}}\right) \times \left(\frac{L_{\text{pl}}}{10^{39}\text{erg/s}}\right) \quad (1)$$

with  $f_{\text{ad},0.3} \approx 1$  is a dimensionless factor quantifying inefficiencies in radiating the recombination energy. We define the plateau as the duration between the point where the transient begins rebrightening after the first blue peak to the time when it falls off the plateau to the same brightness. We calculate an average plateau luminosity  $L_{\text{pl}} \approx 2.3 \times 10^{40} \text{ erg s}^{-1}$  and a plateau duration  $t_{\text{pl}} \approx 274$  days. This suggests a recombining ejecta mass of  $\approx 100 M_{\odot}$  for this LRN, implying an extremely massive progenitor. This seems unlikely, given that the correlation between peak luminosity and progenitor mass for LRNe (Blagorodnova et al. 2021) predicts the primary progenitor mass in the range  $\sim 10 - 50 M_{\odot}$ . Additionally, from archival *HST* imaging Cai et al. (2019) suggest a progenitor mass  $\sim 17 - 24 M_{\odot}$ . It is therefore

very likely that the plateau luminosity is too high to be explained by hydrogen recombination alone. A plausible source of additional energy is shock interaction between the merger ejecta and pre-existing material around the binary that was ejected during the CE phase. Following Matsumoto & Metzger (2022), assuming that only the timescale but not the luminosity of the transient is set by hydrogen recombination, the required recombining ejected mass is

$$t_{\text{pl}} \approx 140 \rho_{i,-11}^{-1/3} \left(\frac{M_{\text{ej}}}{M_{\odot}}\right)^{1/3} \left(\frac{v_E}{300 \text{ km/s}}\right)^{-1} \text{ days} \quad (2)$$

where  $v_E$  is the mean ejecta velocity and  $\rho_{i,-11} = \rho_i / 10^{-11} \text{ g cm}^{-3} \approx 1$  where  $\rho_i$  is the characteristic density at which the recombination completes. We adopt  $v_E \approx 430 \text{ km s}^{-1}$  from Cai et al. (2022) which gives  $M_{\text{ej}} \approx 22 M_{\odot}$ . This value is larger than that derived in Cai et al. (2022) due to the larger plateau duration that we have assumed. Assuming that this ejected mass runs into pre-existing mass ( $M_{\text{pre}} \ll M_{\text{ej}}$ ) with velocity  $v_{\text{pre}} \ll v_E$ , the generated shock luminosity can be written as (Matsumoto & Metzger 2022)

$$L_{\text{pl}}^{\text{sh}} \approx 7 \times 10^{39} \rho_{i,-11}^{-1/3} \left(\frac{M_{\text{pre}}}{0.1 M_{\text{ej}}}\right) \left(\frac{v_E}{300 \text{ km/s}}\right)^3 \left(\frac{M_{\text{ej}}}{M_{\odot}}\right)^{2/3} \text{ erg/s} \quad (3)$$

The observed plateau luminosity can be explained by shock interactions from Eq. 2 and 3 if  $M_{\text{pre}} \approx 0.3 M_{\odot}$ . Given the very late-time bump in the lightcurve of this LRN, it is not unreasonable to expect significant CSM around the binary, providing a plausible explanation for its plateau.

**5. ZTF 21aagppzg (AT 2021blu, Smith et al. 2021b; Pastorello et al. 2022)** is located on the outskirts of the galaxy UGC 5829. It was first classified as an LBV outburst (Uno et al. 2021), however, our late-time NIR spectra show strong molecular absorption features, indicating that this is a LRN. We adopt the extinction to be dominated by the Milky Way, as our early optical spectra do not show any strong Na ID absorption lines.

The lightcurve is characteristic of LRNe and shows two pronounced peaks – an initial blue peak for  $\approx 50$  days, followed by a second red peak lasting for  $\approx 200$  days. Unlike ZTF 21aancgbm, the second peak does not show a plateau but has a smooth rise and decline. The P200/WIRC NIR photometry shows that ZTF 21aagppzg was also significantly brighter in NIR than in the optical. Particularly, at late times when the transient has faded below ZTF detection limits in the *r*-band ( $> 21$  mag), it continues to be detected at  $\approx 17$  mag in the K band (see Fig. 1). We stack the ZTF forced

photometry prior to the outburst in 5-day bins and recover some archival detections. The first detection in  $r$  band is  $\approx 1040$  days prior to peak with  $m_r = 22.3 \pm 0.2$ . The transient was detected again at four epochs in the  $r$  and  $g$  bands between 400 and 300 days before peak, at roughly constant magnitudes of  $m_r = 22.4 \pm 0.3$  and  $m_g = 22.5 \pm 0.3$ . Finally, it is detected again 95 days before peak at  $m_r = 21.8 \pm 0.3$ , brightens to  $m_r = 20.9 \pm 0.2$  65 days before peak and fades back to  $m_r = 21.9 \pm 0.3$  mag at 27 days before peak. It is also detected in the  $i$  band during this time period, with  $m_i = 21.0 \pm 0.3$  mag.

Our spectroscopic coverage comprises four optical spectra at  $-5$ ,  $+6$ ,  $+34$  and  $+54$  days since peak and three NIR spectra at  $+63$ ,  $+301$  and  $+395$  days since peak. The two early-time optical spectra are characterized by a hot blue continuum with strong Balmer emission lines. The  $H\alpha$  emission line has  $v_{\text{FWHM}} \approx 500 - 600 \text{ km s}^{-1}$ . The  $H\beta$  line profile appears to be a superposition of a broad component with a narrow component, however our spectral resolution is not sufficient to distinguish between the two. These spectra do not show the Ca II NIR triplet lines. The third optical spectrum has lower resolution and a lower signal-to-noise ratio (S/N). It shows a reddened continuum, with  $H\alpha$  being the only prominent feature. The final optical spectrum was obtained two months post peak, and shows a reddened continuum. The strength and velocity of the Balmer emission decreased, the  $H\alpha$  line developed a double-peaked profile and the  $H\beta$  is not detected. This spectrum also shows weak Ca II NIR triplet absorption lines, along with a forest of metallic absorption lines. The NIR spectrum at  $+63$  days shows hydrogen emission lines with some metallic absorption lines. Our two final late-time NIR spectra show strong molecular absorption features of TiO, VO and H<sub>2</sub>O.

Similar to ZTF21aancgbm, we can use scaling relations to determine the ejecta masses. We estimate the median luminosity on the red plateau  $L_{\text{pl}} \approx 1.6 \times 10^{40} \text{ erg s}^{-1}$  and a plateau duration  $t_{\text{pl}} \approx 180$  days. Using  $v_E \approx 500 \text{ km s}^{-1}$  and Eq. 2 gives the recombining ejecta mass  $M_{\text{ej}} \approx 10 M_{\odot}$ , although the estimate is very sensitive to the assumed ejecta velocity. Similar to ZTF21aancgbm, the recombination alone is not sufficient to explain the luminosity of the plateau, and Eq. 3 implies interaction with pre-existing mass  $M_{\text{pre}} \approx 0.2 M_{\odot}$ . Pastorello et al. (2022) discuss archival *HST* and ground-based imaging of this transient, and the properties of the putative progenitor. We note that in addition to the data presented in their paper, this transient also has archival *Spitzer Space Telescope*/IRAC imaging from 2007-12-27. We detect a marginal source at the location of the transient with  $m_{3,6} = 20.48 \pm 0.16$

mag and  $m_{4,5} = 19.79 \pm 0.21$  mag (Vega system). We leave a more detailed analysis of this LRN and its progenitor properties to a future study.

**6. ZTF 21acpkzcc (AT 2021aess)** is the most luminous LRN in our sample, with peak  $M_r = -15.12 \pm 0.15$ . We do not identify strong Na ID in our early time spectra, although this is possibly due to low S/N. We assume that the extinction is dominated by the Milky Way, but caution that extinction due to the host galaxy could increase the peak luminosity estimates for this transient. Similar to the other LRNe described above, the lightcurve shows two distinct peaks – a blue initial peak lasting  $\approx 40$  days followed by a reddened plateau. However, our photometric coverage stops at  $\approx 50$  days into the plateau as the transient went into solar conjunction. Similar to the previous two LRNe, ZTF 21acpkzcc is also brighter in the NIR (by  $> 1$  mag) than in the optical bands. Stacking the archival ZTF lightcurve in three day bins shows some archival detections  $\approx 70$  days before peak at  $m_g = 21 \pm 0.3$  and  $m_r = 21.1 \pm 0.3$ . Our spectroscopic coverage comprises three optical spectra at  $+4$ ,  $+46$  and  $+68$  days since peak and one NIR spectrum at  $+54$  days since peak. The early spectra shows narrow  $H\alpha$  with  $v_{\text{FWHM}} \approx 500 \text{ km s}^{-1}$ , which grows weaker and narrower with time ( $\text{FWHM} < 350 \text{ km s}^{-1}$  at 46 days). The  $+68\text{d}$  spectrum also shows a weak P-cygni profile for  $H\alpha$ . The early time spectra also show a forest of Fe II lines and the Ca II NIR triplet lines with P-cygni profiles. The initial blue lightcurve peak with a red plateau together with weakening  $H\alpha$  with time and NIR excess suggest that ZTF21acpkzcc is a LRN. The high luminosity of ZTF 21acpkzcc is similar to the LRN AT 2017jfs (Pastorello et al. 2019b), suggesting a massive binary origin.

We note that two additional LRNe were reported in the last three years – AT 2018bwo (Blagorodnova et al. 2021) and AT 2020kog (Pastorello et al. 2021b). AT 2020kog was missed by ZTF because it landed in the chip-gaps of the ZTF detector. AT 2018bwo was discovered on 2018-05-22, when ZTF was in the reference-building phase. The first ZTF visit to the field of AT 208bwo was two months later on 2018-07-14. No alerts were generated as this field did not have a ZTF reference image. We ran post-facto image subtractions and measured forced PSF photometry and recover two detections of AT 2018bwo in the  $r$  band at  $19.76 \pm 0.08$  and  $20.15 \pm 0.12$  mag on 2018-07-21 and 2018-07-24 respectively.

### 2.2.3. LRN-silver

This category includes two sources that do not show all hallmarks of a LRN, but resemble LRNe in several

aspects. Their lightcurves are plotted in Fig. 1 and their optical and near-infrared spectra are shown in Fig. 2 and 3 respectively.

**1. ZTF 18abwxrhi (AT 2018gzz)** has peak  $M_r = -14.82 \pm 0.17$  and shows two pronounced lightcurve features : a blue first peak followed by a longer lasting red peak/plateau. Our photometric data is sparse for the red peak/plateau as the transient did not brighten significantly above the ZTF sensitivity limits. However, the lightcurve evolution inferred from the available data is strikingly similar to the LRNe in the gold sample. Additionally, a spectrum taken during the first blue peak shows narrow, marginally resolved Balmer emission lines with  $v_{\text{FWHM}} \approx 300 \text{ km s}^{-1}$  ruling out a supernova origin, narrow, unresolved Ca II NIR triplet lines with P-Cygni profiles and narrow Ca II H & K absorption lines. We do not detect Na ID in this spectrum, and hence assume negligible host extinction. There is no spectroscopic coverage at late times. Given these similarities with LRNe, ZTF 18abwxrhi is most likely a LRN, and we include it in the LRN-silver category.

**2. ZTF 21aaeekqd (AT 2021afy)** is located on the outskirts of the galaxy UGC 10043. While Pastorello et al. (2022) classify this transient as a LRN, their late-time spectra do not show obvious molecular absorption features (e.g. as those seen in ZTF 21aancgbm). We also do not identify similar molecular features in any of our spectra. As noted in Pastorello et al. (2022), the lightcurve differs from other LRNe with similar luminosities. For these reasons, we include ZTF 21aaeekqd in our LRN-silver sample. It is possible that obvious molecular features appear at later times, where spectroscopic coverage does not exist.

The transient has a 100-day long lightcurve with two low contrast peaks and is detected only in  $r$  and  $i$  bands by ZTF. In our earliest spectrum, we detect Na ID absorption with equivalent width  $1.8 \pm 0.6 \text{ \AA}$ , consistent with Pastorello et al. (2022). This corresponds to  $E(B-V)_{\text{host}} \approx 0.28 \pm 0.10 \text{ mag}$ , assuming that the interstellar medium is alone responsible for the Na ID absorption. However, we caution that this is unlikely, given the remote location of the transient in the host. It is possible that the sodium absorption originates in circumstellar dust around the progenitor of the explosion, in which case the extinction estimate will be incorrect (Poznancki et al. 2012). Accounting for the Galactic component, we adopt a total  $E(B-V) = 0.33 \pm 0.10 \text{ mag}$ . With this, the transient reaches  $M_{r,\text{peak}} = -13.95 \pm 0.16$ , and is one of the brighter members of our sample. We obtained an epoch of  $J$ -band imaging at +60 days since peak with  $J - r \approx 1 \text{ mag}$ , similar to other LRNe.

Our spectroscopic coverage comprises 3 optical spectra at phases of +33 d, +89 d, +114 d and one NIR spectrum at +92 d since first peak. The +33 day spectrum shows a reddened continuum with narrow  $H\alpha$  ( $v_{\text{FWHM}} \approx 650 \text{ km s}^{-1}$ ) and Ca II NIR triplet in absorption. Of the three Ca II triplet lines, we detect only the 8542 and 8662  $\text{\AA}$  absorption lines. This is likely because the transition probability for the 8498  $\text{\AA}$  line is  $\approx 10$  times smaller than for the other two. Notably, the absorption lines are unresolved, with  $v_{\text{FWHM}} \leq 200 \text{ km s}^{-1}$  (instrumental resolution in this wavelength range is  $v_{\text{inst}} \approx 250 \text{ km s}^{-1}$ , measured from sky emission lines). This velocity is much lower than the  $H\alpha$  photospheric velocity at this phase ( $\approx 650 \text{ km s}^{-1}$ ). These absorption lines likely originate in a dense, slow-moving shell of circumstellar medium outside the photosphere, that was likely ejected prior to the explosion possibly during the CE phase. The +89 day spectrum shows a more reddened continuum with slower, marginally resolved  $H\alpha$  ( $v_{\text{FWHM}} \approx 400 \text{ km s}^{-1}$ ) and narrow  $H\beta$  ( $v_{\text{FWHM}} \approx 300 \text{ km s}^{-1}$ ). The Ca II NIR triplet lines are now seen as a superposition of an emission component with  $v \approx 500 \text{ km s}^{-1}$ , and a central narrow absorption component (see Fig. 5). A possible explanation for this is that the ejecta have crashed into the CSM at this epoch, and the resulting shock has swept up only part of the CSM. A photosphere forms at the shock interface from where the emission lines originate (Ca II predominantly excited by collisions). The narrow, weak absorption component originates from the unshocked CSM shell lying outside the photosphere. The +80 day NIR spectrum shows similar narrow hydrogen emission lines. The spectrum also shows a weak broad feature in the  $H$  band, which is similar to the  $\text{H}_2\text{O}$  absorption seen in ZTF 21aagppzg. The final optical spectrum at +113 d shows a very weak continuum, but extraordinarily strong  $H\alpha$  ( $v_{\text{FWHM}} \approx 300 \text{ km s}^{-1}$ ) and strong, unresolved  $H\beta$  ( $v_{\text{FWHM}} < 400 \text{ km s}^{-1}$ ). The Ca II NIR triplet is seen purely in emission. This suggests that the shock has swept up all the CSM. The Balmer decrement in this spectrum is  $\beta \approx 7$ , supporting that the emission originates in an interaction-dominated region. The absorption to emission transition of the Ca II line profiles suggests that there is a dense, slow-moving shell of CSM around the progenitor. None of the other LRNe in our sample show such a transition. The late-time spectrum with very strong emission lines is unlike the late-time optical spectra of other LRNe in our sample (e.g. ZTF 21aancgbm at 360 days), that show strong molecular absorption bands.

#### 2.2.4. LRN-bronze

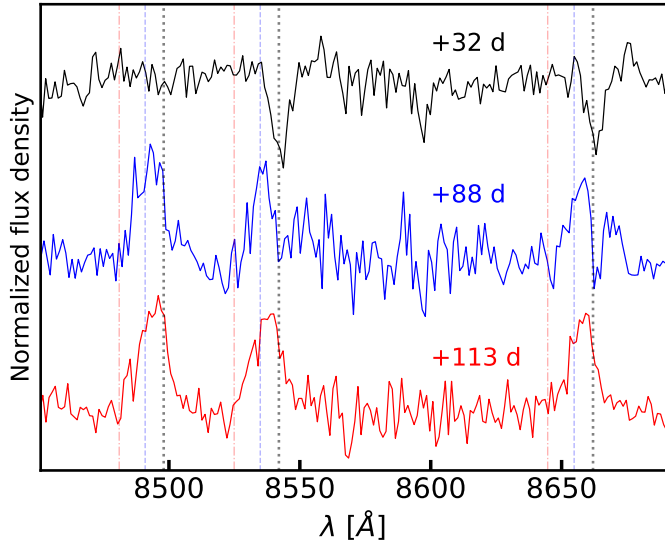


**Figure 5.** Evolution of Ca II line profiles of ZTF 21aaekekq. In the earliest spectrum (+32 d, black), the lines are seen purely in absorption, and likely originate from a shell of slow-moving CSM around the binary. In the second spectrum, the profile has transitioned to emission superposed with a narrow absorption component. This is likely because the ejecta have crashed into the CSM, and swept up only part of the CSM. The shocks in the ejecta produce the emission, while the absorption comes from the unshocked, dense CSM shell outside the photosphere. In the final optical spectrum, the line profiles are pure emission, suggesting that all of the CSM has been swept up by the ejecta.

This category includes three sources - ZTF 18aaajqkmr, ZTF 20abjgdec and ZTF 21aabfwwl that show multiple peaks in their lightcurves but do not have spectroscopic coverage (see Fig. 1). These transients have peak absolute magnitudes of  $-15.36$ ,  $-14.37$  and  $-15.72$ , respectively. ZTF 21aabfwwl was initially classified as a Type II SN (Hinkle 2021), but the spectrum available on TNS is noisy and no H lines are clearly visible. We list these three transients as candidate LRNe.

### 2.2.5. *ILRT-gold*

This category includes six sources that we spectroscopically classify as ILRTs. Their lightcurves are shown in Fig. 6. We calculate the distances and extinction due to the Milky Way as was done for the LRNe (see Sec. 2.2.2). It is challenging to estimate the host galaxy extinctions because ILRTs have extremely dusty progenitors, and often exhibit variable Na I D originating in outflows (Cai et al. 2021; Smith et al. 2009, also see discussion of ZTF 19acoaiub below). Instead, we use the peak optical  $g - r$  colors of ILRTs to estimate the host extinction, similar to Humphreys et al. (2011); Smith et al. (2009); Jencson et al. (2019). The spectra of ILRTs

at peak show F-type absorption features, suggesting  $T \approx 7500$  K. Cai et al. (2021) find that the ILRTs in their sample have peak  $B - V$  colors in the range  $0.2 - 0.4$  mag, consistent with this interpretation. We use the peak colors of the ILRTs in our sample to estimate the value of  $E(B - V)_{\text{host}}$  required to bring the colors in this range. We estimate a non-negligible extinction for two ILRTs in our sample -  $E(B - V) \approx 0.7$  for ZTF 19aadyppr (consistent with Jencson et al. 2019) and  $E(B - V) \approx 0.2$  for ZTF 19aagqkrq. For the other transients, we assume the extinction to be dominated by the Galactic component. We calculate pseudo-bolometric luminosities by fitting blackbodies to the available data. Table 3 lists the derived photometric properties of the ILRTs. Our optical and NIR spectra for these transients are shown in Figs. 7 and 8. Similar to the LRNe, we derive line velocities by fitting Lorentzian line profiles and list the derived values in Table 4. We briefly discuss the properties of the transients here.

Two of these transients - ZTF 19aadyppr and ZTF 21aclzzex have spectroscopic coverage extending to late times. Of these, ZTF 19aadyppr is in the galaxy M 51 and has been studied in detail by Jencson et al. (2019), who identified its red, dusty progenitor. The object shows a single-peaked red lightcurve, and its spectra show narrow  $H\alpha$  and [Ca II] emission, characteristic of ILRTs.

ZTF 21aclzzex is the brightest ILRT in our sample, with peak  $M_r = -15.68 \pm 0.16$  mag. Our lightcurve coverage is sparse and noisy, but the available data shows indications that the transient is red, and possibly has multiple peaks. However, our spectroscopic coverage extends to 163 days since peak, and resembles the evolution of ILRTs. An early time spectrum at 9 days since peak shows a blue continuum with narrow  $H\alpha$ ,  $H\beta$ , Ca II and [Ca II] emission. The spectrum also shows Ca II H & K absorption. The next optical spectrum obtained at 84 d since peak shows a reddened continuum with narrow  $H\alpha$ , Ca II, [Ca II] emission and Ca II H & K absorption. [O I] is detected as a weak emission line. The 118 d optical spectrum shows similar features, except the [O I] has become stronger. Similar [O I] emission was observed in the ILRT AT 2013la (Cai et al. 2021). The 134 d NIR spectrum shows strong, narrow hydrogen emission lines, He I and O I emission. Although the lightcurve is not informative enough to classify the transient, the spectroscopic evolution is strikingly similar to several ILRTs, especially with [Ca II] emission seen consistently in all spectra. For this reason, we classify it as an ILRT.

The other four transients have only early-time spectroscopic coverage. Analogous to the other ILRTs, they all show narrow  $H\alpha$  and [Ca II] emission in their spectra.

**Table 3.** Photometric properties of LRN and ILRTs<sup>a</sup>

Name	DM <sup>b</sup> (mag)	E(B-V) <sup>c</sup> (mag)	m <sub>r,peak</sub> (mag)	M <sub>r,peak</sub> (mag)	MJD <sub>peak</sub> (d)	L <sub>peak</sub> (erg s <sup>-1</sup> )
ZTF18acbwfza	31.60	0.250	18.47 ± 0.02	-13.82 ± 0.15	58430.9 ± 0.2	9.3 <sup>+0.3</sup> <sub>-0.3</sub> × 10 <sup>40</sup>
ZTF19adakuot	24.45	0.055	15.00 ± 0.01	-9.60 ± 0.15	58891.6 ± 0.1	2.0 <sup>+0.1</sup> <sub>-0.1</sub> × 10 <sup>39</sup>
ZTF20aawdwch	28.97	0.093	17.79 ± 0.02	-11.43 ± 0.15	58963.0 ± 1.2	> 1.2 × 10 <sup>40</sup>
ZTF21aagppzg	29.90	0.020	16.45 ± 0.01	-13.50 ± 0.15	59258.9 ± 0.1	7.9 <sup>+0.1</sup> <sub>-0.1</sub> × 10 <sup>40</sup>
ZTF21aancgbm	29.43	0.261	16.28 ± 0.03	-13.86 ± 0.15	59252.9 ± 0.5	> 8.9 × 10 <sup>40</sup>
ZTF21acpkzcc	32.09	0.032	17.05 ± 0.03	-15.12 ± 0.15	59545.5 ± 0.2	3.3 <sup>+0.2</sup> <sub>-0.2</sub> × 10 <sup>41</sup>
ZTF18abwxrhi	33.70	0.047	19.33 ± 0.06	-14.50 ± 0.16	58386.2 ± 0.9	1.9 <sup>+1.5</sup> <sub>-0.3</sub> × 10 <sup>41</sup>
ZTF21aaekeqd	32.87	0.330	19.82 ± 0.06	-13.95 ± 0.16	59229.2 ± 1.6	6.0 <sup>+6.4</sup> <sub>-4.6</sub> × 10 <sup>41</sup>
ZTF18aajpgmr	35.00	0.018	19.69 ± 0.09	-15.36 ± 0.17	58969.7 ± 1.0	3.3 <sup>+0.7</sup> <sub>-0.4</sub> × 10 <sup>41</sup>
ZTF20abjgdec	33.78	0.141	19.80 ± 0.06	-14.37 ± 0.16	59045.6 ± 2.1	2.4 <sup>+13.3</sup> <sub>-1.2</sub> × 10 <sup>41</sup>
ZTF21aabfwwl	33.99	0.043	18.39 ± 0.05	-15.72 ± 0.16	59239.5 ± 1.8	5.2 <sup>+1.1</sup> <sub>-0.7</sub> × 10 <sup>42</sup>
ZTF18acdyopn	33.92	0.064	19.76 ± 0.11	-14.33 ± 0.19	58426.8 ± 2.4	2.2 <sup>+21.7</sup> <sub>-1.0</sub> × 10 <sup>41</sup>
ZTF19aadyppr	29.45	0.705	16.65 ± 0.01	-14.73 ± 0.15	58534.7 ± 0.5	2.3 <sup>+0.1</sup> <sub>-0.1</sub> × 10 <sup>41</sup>
ZTF19acoaiub	31.83	0.038	17.31 ± 0.02	-14.62 ± 0.15	58799.1 ± 0.1	2.0 <sup>+0.2</sup> <sub>-0.2</sub> × 10 <sup>41</sup>
ZTF19acdrkbh	34.33	0.051	19.85 ± 0.12	-14.62 ± 0.20	58764.3 ± 1.9	1.8 <sup>+0.9</sup> <sub>-0.4</sub> × 10 <sup>41</sup>
ZTF19aagqkrq	30.76	0.200	17.58 ± 0.03	-13.72 ± 0.15	58538.3 ± 1.1	8.0 <sup>+0.5</sup> <sub>-0.4</sub> × 10 <sup>40</sup>
ZTF21aclzzex	33.89	0.019	18.26 ± 0.06	-15.68 ± 0.16	59528.6 ± 1.7	5.2 <sup>+3.7</sup> <sub>-1.2</sub> × 10 <sup>41</sup>
ZTF21abtduah	33.22	0.022	< 18.31	< -14.96 ± 0.15	< 59522.5	> 1.3 × 10 <sup>41</sup>
ZTF21abfxjld	33.43	0.106	< 19.51	< -14.21 ± 0.20	< 59359.8	> 8.0 × 10 <sup>40</sup>
ZTF19aavwbxs	33.26	0.038	18.92 ± 0.08	-14.44 ± 0.17	58644.7 ± 8.1	2.2 <sup>+0.6</sup> <sub>-0.3</sub> × 10 <sup>41</sup>
ZTF18acrykgg	33.35	0.036	< 19.31.	< -14.14 ± 0.16	< 58447.5	

*a* : The two classes LRN and ILRT are separated by a horizontal line.

*b* : The distance moduli have uncertainties of 0.15 mag and are taken from NED.

*c* : Galactic extinction values are taken from [Schlafly & Finkbeiner \(2011\)](#); host extinction is calculated as described in the text.

We note that while the LRN AT 2018hso also showed [Ca II] emission in its early spectra, it also had two pronounced peaks in its lightcurve. None of these four transients show multiple peaks and are not AT 2018hso-like LRNe. We thus classify them as ILRTs based on narrow H $\alpha$ , [Ca II] emission and lack of multi-peaked lightcurves.

Of these four, ZTF 19acoaiub (AT 2019udc) and ZTF 19aagqkrq (AT 2019ahd) have the best sampled lightcurves. ZTF 19acoaiub is located in NGC 718 and has peak  $M_r = -14.68 \pm 0.04$  mag, a relatively fast declining single-peaked lightcurve. The ZTF lightcurve also samples the pre-peak rise. 7 days before peak, the transient was extremely red with  $g - r \approx 0.8$  mag. As it brightens, the transient also evolves to bluer colors of  $g - r \approx 0.4$  mag five days before peak and  $g - r \approx 0.2$  mag at peak. The transient then declines at a rate of  $\approx 0.03$  mag day<sup>-1</sup> for the next 60 days as it evolves back to redder colors. Our only optical spectrum was obtained 7 days before the peak and shows strong H $\alpha$  emission with  $v_{\text{FWHM}} \approx 1300$  km s<sup>-1</sup>. This spectrum also shows nar-

row Ca II and [Ca II] emission features, similar to several other ILRTs. This pre-peak spectrum shows very strong Na I D absorption with  $\text{EW} \approx 4.8 \pm 0.7$  Å consistent with its pre-peak red colors. A likely explanation for this behaviour is that the progenitor of ZTF 19acoaiub was dust enshrouded. This circumstellar dust was destroyed by the explosion, causing the transient to evolve to bluer colors as it brightened. This transient demonstrates the issue with using early-time Na I D features to estimate the host extinction.

ZTF 19aagqkrq (AT 2019ahd) has peak  $M_r = -13.72 \pm 0.15$  mag and has a blue color up to a few days before peak but rapidly transitions to red colors. Our spectroscopic coverage comprises two optical spectra obtained on successive nights at peak and 1 day post-peak. Both spectra show H $\alpha$  emission with  $v_{\text{FWHM}} \approx 700$  km s<sup>-1</sup> and strong Ca II and [Ca II] emission lines.

The remaining two – ZTF 18acdyopn and ZTF 19acdrkbh – have relatively sparse lightcurve sampling. ZTF 18acdyopn has a peak absolute magnitude  $M_r = -14.33 \pm 0.19$  mag and declines by 1.5 mag in the  $r$  band in 80 days. Al-

though our lightcurve does not sample the peak, the available data shows that the transient had red colors a few days post-peak. An optical spectrum taken five days since peak shows narrow hydrogen Balmer emission lines ( $v_{\text{FWHM}} \approx 300 \text{ km s}^{-1}$ ), [Ca II], Ca II H & K as well as Ca II NIR triplet emission lines. Similarly, ZTF 19acdrkbh has peak  $M_r = -14.62 \pm 0.15$ , and was detected at the threshold of ZTF sensitivity, and has  $g - r \approx 0.6$  mag at peak. An optical spectrum at +19 days since peak shows narrow  $H\alpha$  ( $v_{\text{FWHM}} \approx 600 \text{ km s}^{-1}$ ) and possible Na I D absorption, similar to other ILRTs.

### 2.2.6. *ILRT-silver*

This category includes two sources – ZTF 21abtduah and ZTF 21abfxjld – that show luminosities and spectral evolution broadly similar to ILRTs, but do not have [Ca II] emission. Although [Ca II] emission in ILRTs is a sign of interaction with the surrounding circumstellar material (CSM), its strength is sensitive to the CSM density (Humphreys et al. 2011). For example, the proposed ILRT AT 2019krl did not show Ca II emission in several of its spectra (Andrews et al. 2021).

For both transients, our lightcurve coverage does not sample the peak, and it is not clear whether they have multiple peaks. For ZTF 21abtduah, our lightcurve samples the brightening and fading of the transient (see Fig. 6). We estimate a fiducial peak time by fitting a polynomial to these points. For ZTF 21abfxjld, the ZTF lightcurve samples the fading of the lightcurve. However, the ATLAS *o*-band lightcurve shows two measurements separated by 5 days that do not show significant evolution, suggesting that the transient peaked around then. We determine the peak time by fitting a polynomial to the ATLAS *o*-band lightcurve. We have late-time spectroscopic coverage for both these transients. In a spectrum taken 24 days since the (fiducial) peak, ZTF 21abtduah shows  $H\alpha$  with  $v_{\text{FWHM}} \approx 1200 \text{ km s}^{-1}$ . A second spectrum obtained at 48 days since peak shows a double-peaked  $H\alpha$  profile, suggesting interaction with slow moving CSM, or absorption in an external shell. This spectrum also shows narrow Ca II NIR triplet in emission. The final spectrum taken at 140 days since peak shows strong  $H\alpha$ ,  $H\beta$ , Ca II NIR and O I emission lines, similar to ZTF 21aclzzex and AT 2013la (however [Ca II] lines are not seen). The  $H\alpha$  line profile in this spectrum is also double-peaked. ZTF 21abfxjld has spectra at +44d and 83 days since peak, both of which show  $H\alpha$  emission with  $v_{\text{FWHM}} \leq 300 \text{ km s}^{-1}$ , and narrow [Ca II] emission. We also have two NIR spectra taken at +26 d and +125 d since peak. The 26 day NIR spectrum shows narrow H emission lines. However, the

**Table 4.** Spectroscopic properties of LRNe and ILRTs

Name	MJD (d)	Phase (d)	$v_{\text{H}\alpha, \text{FWHM}}^a$ ( $\text{km s}^{-1}$ )	$v_{\text{H}\beta, \text{FWHM}}^a$ ( $\text{km s}^{-1}$ )	$\beta$
LRNe					
ZTF18acbwfza	58424	-7.1	$510 \pm 60$		
ZTF18acbwfza	58424	-7.1	$450 \pm 30$	$750 \pm 60$	$2.1 \pm 0.1$
ZTF18acbwfza	58432	+0.9	$350 \pm 40$	$760 \pm 120$	$2.2 \pm 0.2$
ZTF18abwrxrhi	58379	-9.3	$280 \pm 40$	$250 \pm 120$	$3.8 \pm 0.7$
ZTF21aaekeqd	59262	+33.4	$650 \pm 20$		
ZTF21aaekeqd	59318	+89.3	$340 \pm 30$	$260 \pm 70$	$2.1 \pm 0.2$
ZTF21aaekeqd	59343	+113.8	$300 \pm 20$	$< 370$	$7.6 \pm 0.6$
ZTF21aagppzg	59253	-5.9	$490 \pm 60$	$760 \pm 100$	$2.5 \pm 0.2$
ZTF21aagppzg	59265	+6.1	$420 \pm 40$	$700 \pm 80$	$2.7 \pm 0.2$
ZTF21aagppzg	59313	+54.1	$500 \pm 60$		
ZTF21aanegbm	59313	+60.1	$< 350$		
ZTF21aanegbm	59613	+360.1	$460 \pm 40$		
ZTF21acpkzcc	59549	+4.6	$470 \pm 50$	$540 \pm 70$	$3.7 \pm 0.3$
ZTF21acpkzcc	59591	+46.6	$< 340$		
ZTF21acpkzcc	59613	+68.6	$< 300$		
ILRTs					
ZTF18acdypn	58432	+5.1	$300 \pm 40$	$630 \pm 120$	$3.3 \pm 0.4$
ZTF19aadyppr	58509	-25.7	$330 \pm 50$	$< 250$	$2.5 \pm 0.3$
ZTF19aadyppr	58526	-8.7	$640 \pm 80$	$680 \pm 180$	$2.4 \pm 0.4$
ZTF19aadyppr	58537	+2.2	$470 \pm 170$	$2400 \pm 850$	$0.9 \pm 0.3$
ZTF19aadyppr	58549	+14.3	$530 \pm 120$		
ZTF19aadyppr	58558	+23.2	$710 \pm 180$		
ZTF19aadyppr	58586	+51.3	$400 \pm 70$		
ZTF19aadyppr	58616	+81.3	$330 \pm 40$		
ZTF19acoaiub	58792	-7.1	$1250 \pm 300$	$2000 \pm 850$	$3.4 \pm 1.1$
ZTF19acdrkbh	58783	+18.7	$590 \pm 80$		
ZTF19aagqkrq	58525	-13.4	$< 850$	$1000 \pm 200$	$2.3 \pm 0.3$
ZTF19aagqkrq	58526	-12.4	$670 \pm 50$	$2000 \pm 500$	$1.6 \pm 0.2$
ZTF21aclzzex	59530	+1.9	$670 \pm 60$	$1200 \pm 180$	$3.5 \pm 0.5$
ZTF21aclzzex	59605	+76.9	$500 \pm 60$	$380 \pm 110$	$5.5 \pm 1.9$
ZTF21aclzzex	59639	+110.3	$550 \pm 40$	$300 \pm 70$	$7.9 \pm 0.9$
ZTF21abtduah	59524	+1.5	$1170 \pm 100$		
ZTF21abtduah	59549	+26.5	$1290 \pm 100$		
ZTF21abtduah	59613	+90.5	$870 \pm 30$	$690 \pm 70$	$8.4 \pm 0.6$
ZTF21abtduah	59641	+118.5	$770 \pm 30$	$780 \pm 60$	$10.6 \pm 0.6$
ZTF21abfxjld	59401	+41.7	$< 290$	$< 250$	$3.6 \pm 0.5$
ZTF21abfxjld	59440	+80.2	$< 270$	$< 260$	$4.6 \pm 0.4$

The velocities have been corrected for instrumental resolutions listed in Table 2. Upper limits are reported for unresolved lines.



125 day spectrum shows strong but narrow H and He absorption in the  $J$  band. Such features are not seen in any other ILRTs.

The low expansion velocities of these transients argue against a core-collapse SN origin for them. The lack of any molecular features at late times rules out LRNe. None of them show any significant outbursts in archival data. The nature of these transients is not completely clear. Their spectral features point towards CSM interaction. The lack of Ca II emission suggests that the CSM is denser than in typical ILRTs. These transients could represent a peculiar variety of ILRTs. For these reasons, we classify these as ILRT-silver sources.

### 2.2.7. ILRT-bronze

This category includes two sources ZTF 19aavwxbs and ZTF 18acrygkg. ZTF 19aavwxbs shows a single peak lasting 20 days in the ZTF and ATLAS lightcurve before it went into solar conjunction. A low resolution ( $R \sim 100$ ) spectrum of ZTF 19aavwxbs taken with the Spectral Energy Distribution Machine (SEDM; Blagorodnova et al. 2018; Rigault et al. 2019) spectrograph on the 60-inch telescope at Palomar Observatory shows H $\alpha$  emission with  $v_{\text{FWHM}} \leq 3000 \text{ km s}^{-1}$ . No other features are discernible in the spectrum. ZTF 18acrygkg has a lightcurve lasting for 40 days in the ZTF data. There is no spectroscopic data for ZTF 18acrygkg. It is possible that both these transients are low-luminosity Type II SNe so we only list them as ILRT candidates.

### 2.2.8. Ambiguous sources

Finally, we have seven sources that do not have spectroscopic coverage and the photometric data is not enough to determine a tentative classifications. Most of these sources are likely supernovae where the ZTF data samples the late-time phases. The  $5\text{-}\sigma$  alert lightcurves of these transients have durations shorter than 25 days.

## 3. VOLUMETRIC RATE

To estimate the volumetric rates, we simulate the ZTF survey from 2018-06-01 to 2022-02-20 with the python package `simsurvey` (Feindt et al. 2019) using the ZTF pointing history and actual ZTF difference images to estimate the limiting magnitudes of each pointing. Using template lightcurves, we then inject LRNe and ILRTs for a range of possible rates and identify the number of transients that would be detected by the selection criteria of our experiment. Comparing simulations to the observed LRN/ILRT sample gives a first estimate of the rate. This estimate is then corrected for selection effects such as the spectroscopic completeness of the CLU experiment and the CLU galaxy catalog.

### 3.1. Template lightcurves

LRNe exhibit a dichotomy in their lightcurves. The brighter LRNe ( $M_r \geq -11$ ) are characterized by a double peaked lightcurve, while the lower luminosity events have a single peak and much shorter durations (Blagorodnova et al. 2021; Pastorello et al. 2019a). All except one of the ZTF events are brighter than  $-11$  mag, and have double-peaked lightcurves lasting for  $\sim 150$  days. ZTF 19adakuot with  $M_{r,\text{peak}} \approx -9.5$  is the least luminous event in our sample and fades quicker than any of the other events. Owing to the different lightcurve shapes and durations of the brighter LRNe and the fact that most of the ZTF LRNe belong to this category, we restrict our rate analysis to events with  $M_r$  brighter than  $-11$  mag.

We created an empirical LRN lightcurve template using the three well-sampled LRNe in our sample with  $M_{r,\text{peak}} \leq -11$  and two double-peaked LRNe from the literature AT 2017jfs (Pastorello et al. 2019b) and AT 2020kog (Pastorello et al. 2021b). We first normalized the  $g$  and  $r$ -band lightcurves by their peak magnitude in the respective filter. We then fit a Gaussian Process model with a radial basis function (RBF) kernel to the normalized lightcurve. The  $g$  and  $r$ -template lightcurves of the LRNe are shown in the top row of Fig. 9, and provided online.

The lightcurves of ILRTs are more homogeneous than LRNe. We construct lightcurve templates using  $g$  lightcurves of 4 ILRTs (AT 2018aes, AT 2019abn, AT 2019udc and AT 2019ahd) and  $r$ -band lightcurves of these and 4 additional ILRTs (AT 2010dn, AT 2012jc, AT 2013la and AT 2013lb). The ILRT templates are shown in the bottom row of Fig. 9. Both LRN and ILRT template lightcurves are available online (Sec. 7).

### 3.2. Luminosity Function

In this paper, we have presented the first controlled sample of LRNe and ILRTs from a systematic survey. We use this sample to calculate the luminosity function of LRNe and ILRTs.

We restrict ourselves to all gold and silver LRNe that have peak absolute magnitudes brighter than  $-11$ . Fig. 10 shows a histogram of the peak absolute magnitudes of the events in the ZTF sample. As the events are detectable out to different volumes (all smaller than the CLU volume limit of 200 Mpc), the histogram needs to be volume corrected to determine an accurate luminosity function. The volume corrected distribution of peak absolute magnitudes of LRNe in our sample is plotted in Fig. 10 with a different color. Each event has been weighted by  $\frac{1}{V_{\text{max}}}$  where  $V_{\text{max}}$  is the maximum volume out to which that event can be detected

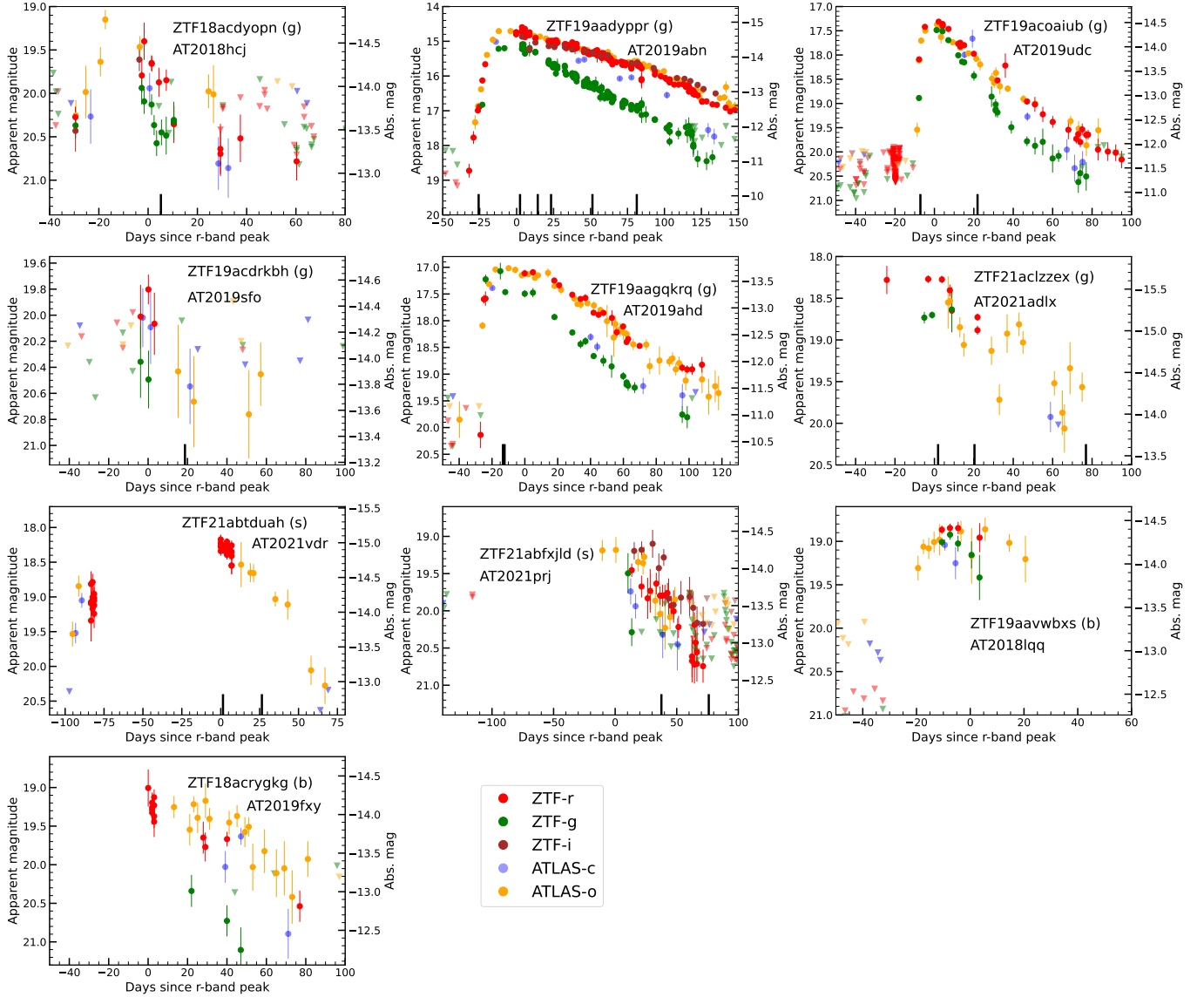


**Figure 6.** Forced photometry lightcurves of the 10 ILRTs in our sample. The transients in gold, silver and bronze samples are marked in parentheses with g, s and b respectively. The ZTF-g, ZTF-r, ZTF-i, ATLAS-c and ATLAS-o band datapoints are plotted in green, red, brown, blue and orange circles respectively. Downward pointing triangles indicate  $5\text{-}\sigma$  upper limits. The days are in observer frame. The lightcurves have been corrected for extinction using the values listed in Table 3. Solid black vertical lines indicate epochs at which the spectra were obtained.

( $V_{\max} \propto 10^{\frac{3}{5}(20-M_{r,\text{peak}})}$ ). The volume corrected distribution shows a steep decline of the event rate with increasing peak luminosity. Fig. 10 also shows the distribution of the ZTF events combined with events from literature (taken from Blagorodnova et al. 2021). The distribution of the ZTF events is broadly consistent with that of the ZTF+literature events (although there are significant biases associated with the literature sample). The peak-luminosity distribution of ZTF events is well-fit by a straight line (in log-space) with a slope  $0.6 \pm 0.1$ . This corresponds to  $\frac{dN}{dL} \propto L^{-2.5 \pm 0.3}$ . This is significantly steeper than the luminosity function de-

rived for low luminosity ( $M_V > -10$ ) LRNe (Kochanek et al. 2014). The implications of these differences are discussed in Sec. 4.1.

Similarly, we calculate the ILRT luminosity function using the 8 gold and silver events from our sample. Fig. 10 (right panel) shows the volume-corrected distribution of the peak absolute magnitudes of ZTF ILRTs. We fit a straight line with slope  $0.6 \pm 0.2$  to the distribution (in log-space), for  $M_r < -13.5$ . This corresponds to a luminosity function of  $\frac{dN}{dL} \propto L^{-2.5 \pm 0.5}$ . This scaling only samples the brighter end of the ILRT luminosity function. Fig. 10 also shows the distribution of pre-

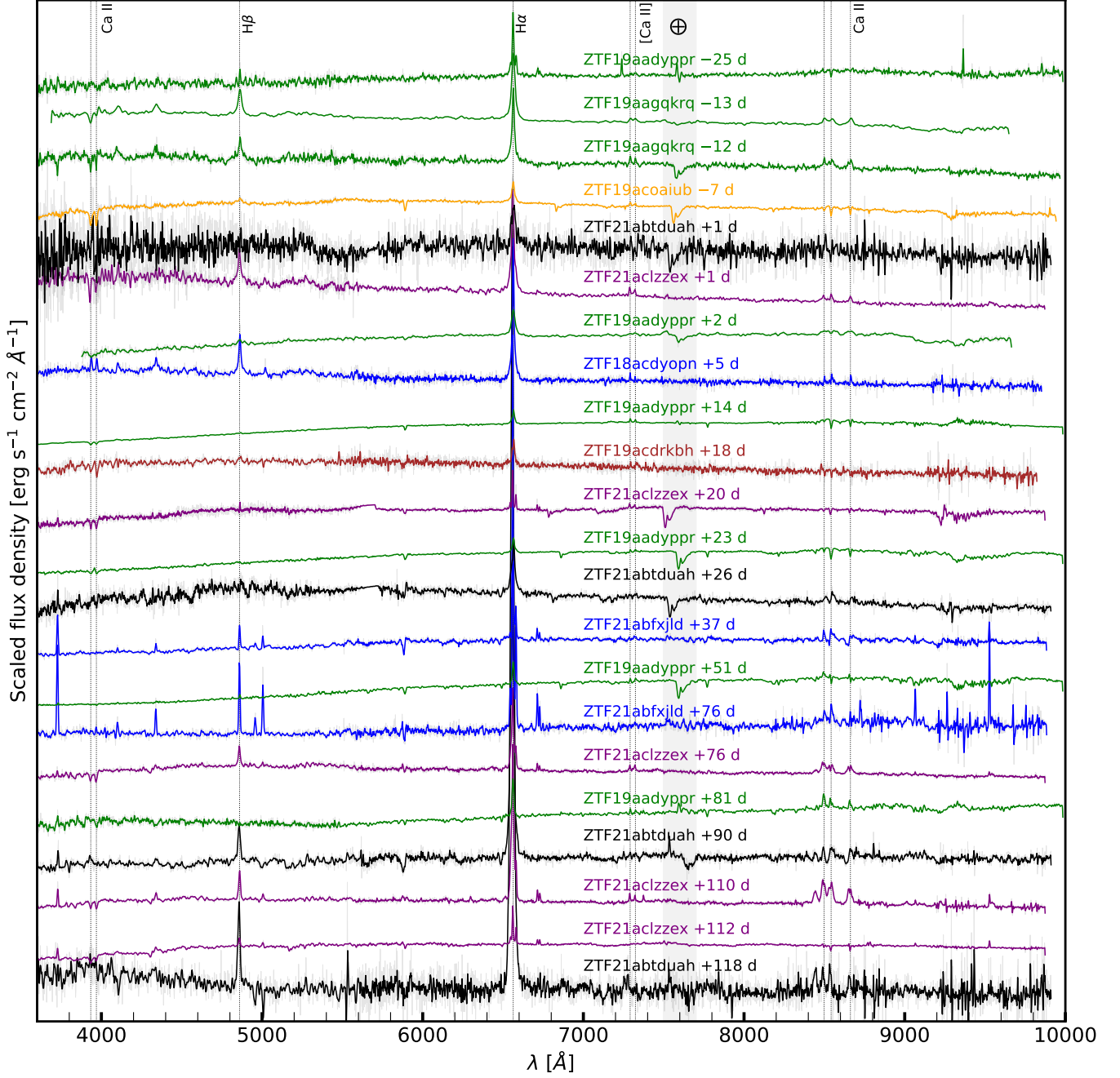


**Figure 7.** Optical spectra for ILRTs presented in this paper.

viously known events from literature together with the ZTF sample, which extends to lower luminosities than the ZTF sample ( $M_r \approx -12$ ). We note that for both LRNe and ILRTs, including the bronze or excluding the silver sample does not significantly change the derived luminosity function.

### 3.3. Sub-sample for rate estimates

We build a sub-sample from the candidates listed in Table 1 to use for rate calculations. All sources listed

as potential LBVs are naturally excluded. To exclude the “ambiguous” transients, we introduce an additional selection criterion – a minimum threshold of 25 days on the duration of the ZTF lightcurve (i.e. the  $5\text{-}\sigma$  detections in  $g$  or  $r$  bands should span at least 25 days). Of the remaining sources, we only include those transients that have spectroscopic coverage (i.e. the gold and silver categories) to obtain an estimate of the rate, as this estimate is subsequently corrected for spectroscopic com-

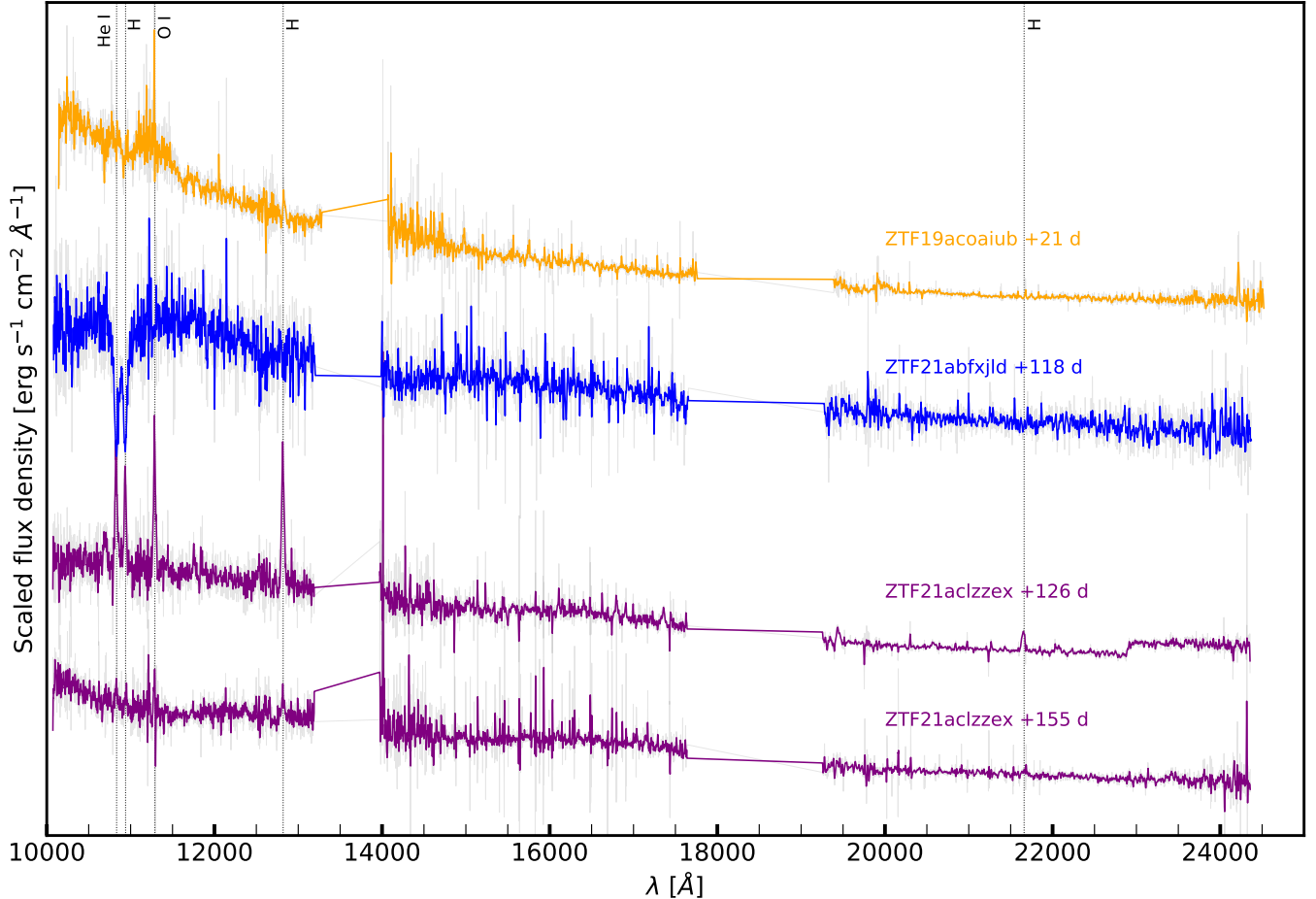


**Figure 8.** NIR spectra for ILRTs presented in this paper.

pletteness. The sub-sample used for rate calculations is marked with an asterisk in Table 1.

The LRN sub-sample used for rate estimates comprises seven out of the eight gold and silver LRNe from Table 1. ZTF 19adakuot is excluded because of its low luminosity (Sec. 3.2). As noted in Sec. 2.2.2, the LRNe AT 2018bwo and AT 2020kog were not detected in the ZTF alert stream. Two detections of AT 2018bwo were recovered post-facto, but it is excluded by the lightcurve-duration criterion. AT 2020kog is excluded because it was in the chip-gaps of the ZTF camera, an effect that is accounted for by our survey simulations. The ILRT sub-sample comprises five out of the eight gold and silver ILRTs. The remaining three do not satisfy the lightcurve duration criterion.

#### 3.4. Volumetric Rates

The luminosity functions and template lightcurves were used to simulate LRNe and ILRTs, and the `sim-survey` simulations of the ZTF survey were used to count how many of them would be detected by our experiment. We apply the selection criteria described in

Sec. 2.1 and the lightcurve-duration criterion from Sec. 3.3 to the simulated transients. We conduct 100 iterations of simulations for each rate to estimate the median and 1- $\sigma$  errors on the number of transients recovered for each rate.

The top-left panel of Fig. 11 shows the number of LRNe that would be detected by our selection criteria as a function of their volumetric rate. The top-right panel of Fig. 11 shows a histogram of the fraction of simulations where the number of detected simulated transients equals the observed number of seven LRN-gold and LRN-silver events. We fit the distribution with a skewed gaussian function to estimate the median and 68 percentile confidence limits. Accounting for an additional poisson uncertainty associated with the seven observed events we derive a volumetric rate of  $r_{\text{LRN,u}} = 5.7^{+4.4}_{-2.7} \times 10^{-5} \text{ Mpc}^{-3} \text{ yr}^{-1}$ .

This estimate does not account for four factors which may result in underestimation compared to the true LRN rate – 1) the CLU experiment is limited to 100'' or 30 kpc from nuclei of galaxies and will miss farther transients, 2) the CLU experiment is not 100% spectroscopi-

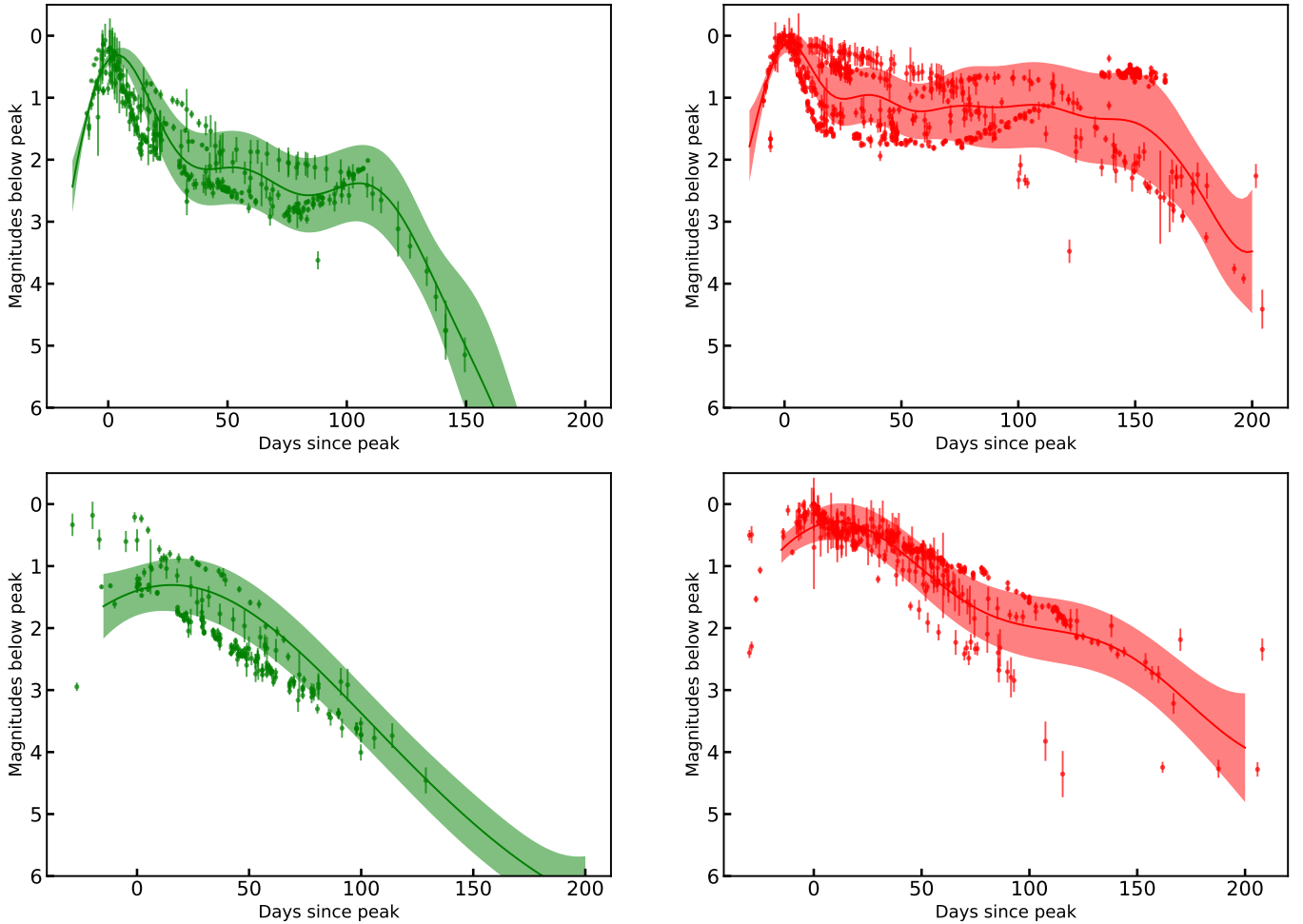


**Figure 9.**  $g$  and  $r$  band lightcurve templates (green and red colors respectively) for LRNe (top row) and ILRTs (bottom row). The solid points depict lightcurves of transients that were used to build the templates. The line and shaded regions show the templates and 68% uncertainties derived from Gaussian Process fits to the transients. The templates capture the essence of the photometric evolution of LRNe (initial blue peak + long lived second peak/plateau) and ILRTs (single peak, red lightcurve). These templates are available online (see Sec. 7).

cally complete, 3) the CLU experiment relies on the CLU galaxy catalog and is affected by its completeness, and 4) some LRNe will be missed due to inefficiencies of the ZTF image subtractions pipeline. First, we note that all literature events have been discovered within  $100''$  or  $140$  kpc of their respective hosts. We searched through transients classified as part of the ZTF BTS – an all-sky, magnitude limited survey with ZTF and did not find any additional LRNe. For this reason, we believe that the CLU offset criterion does not have a significant effect on the rate estimate. Second, the CLU experiment is  $\approx 80\%$  spectroscopically complete for  $m_r < 20$  mag transients. This suggests that the completeness corrected rate is  $7.1^{+5.9}_{-3.4} \times 10^{-5} \text{ Mpc}^{-3} \text{ yr}^{-1}$ . However, the CLU completeness is a function of apparent magnitude, and varies from 100% for  $m_r < 18$  mag, 95% for  $m_r < 19$  mag. To account for this, we calculate the completeness

as a function of apparent magnitude in bins of 1 mag. For each simulation of each of our rates, we bin the simulated transients by peak apparent magnitude, and count only the fraction of events that would be classified based on the CLU criteria. This exercise gives a value consistent with the simplified approach described above. This is because a majority of the events have faint apparent magnitudes, and the (large) uncertainties on this estimate are dominated by low number statistics.

Third, to correct for the incompleteness of the galaxy catalog, we used the redshift completeness factor (RCF) derived from the BTS. As all events in our sample come from starforming galaxies, we calculate the RCF for starforming galaxies in the BTS sample as a function of redshift ( $z$ ) and WISE  $3.36 \mu\text{m}$  absolute magnitude ( $M_{W1}$ ) as described in Fremling et al. (2020). We then use the redshifts and  $M_{W1}$  magnitudes of the host galaxy

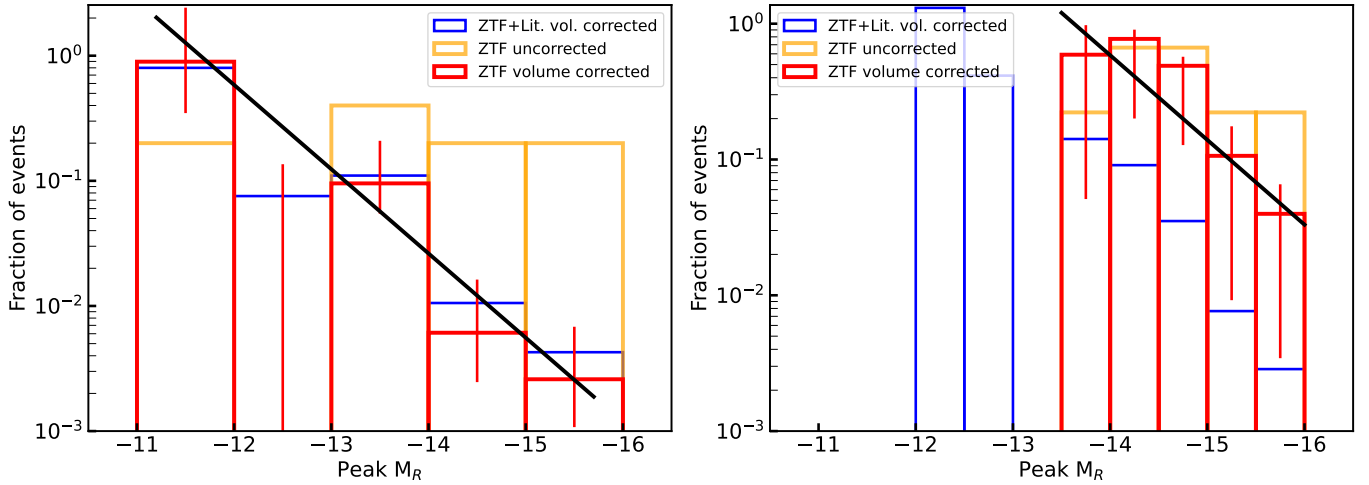


**Figure 10.** Distribution of the peak absolute magnitudes of LRNe (*left*) and ILRTs (*right*) in our sample. The volume corrected ZTF sample with Poisson errorbars is shown in red, and the volume corrected ZTF+literature sample is shown in blue. The black line shows a linear fit to this data (in log-space). We derive a luminosity scaling  $dN/dL \propto L^{-2.5 \pm 0.3}$  for LRNe and  $dN/dL \propto L^{-2.5 \pm 0.5}$  for ILRTs.

ies of LRNe in our sample and weight each event by  $\frac{1}{RCF(z, M_{W1})}$  to estimate the effect of galaxy catalog incompleteness. We find that this leads to an underestimation of the rate by  $\approx 10\%$ .

Finally, the ZTF image subtraction pipeline has two possible sources of inefficiency that are relevant for this calculation. In each science image, the pipeline actively masks pixels that are affected by quality cuts (e.g. saturation due to high brightness, cosmic rays, bad pixels). This introduces a time-dependent source of incompleteness. This dynamic masking does not have a significant effect as LRNe and ILRTs have long durations and are picked up by the pipeline eventually. A more serious issue pertains to the reduced efficiency of the image subtraction algorithm on bright galaxy backgrounds, as are common for the LRNe and ILRTs in our sample. The ZTF pipeline efficiency as a function of background brightness has not been studied to date, and this analysis is outside the scope of this paper. We therefore caution that our rates are possibly lower limits. Applying the corrections described above (except pipeline efficiency), we derive a corrected rate of  $r_{\text{LRNe}} = 7.8^{+6.5}_{-3.7} \times 10^{-4} \text{ Mpc}^{-3} \text{ yr}^{-1}$  for LRNe.

Similarly, using the ILRT luminosity function and `simsurvey` simulations, we derive an uncorrected rate  $r_{\text{ILRT,u}} = 1.9^{+1.3}_{-1.0} \times 10^{-6} \text{ Mpc}^{-3} \text{ yr}^{-1}$  (see bottom panel of Fig. 11). Correcting for the incompleteness effects described above gives  $r_{\text{ILRT}} = 2.6^{+1.8}_{-1.4} \times 10^{-6} \text{ Mpc}^{-3} \text{ yr}^{-1}$ .

## 4. DISCUSSION

### 4.1. LRNe

Kochanek et al. (2014) used three Galactic mergers to estimate the rate of low luminosity stellar mergers with

$M_V \geq -10$  mag. They find that the luminosity function of these mergers is roughly  $\frac{dN}{dL} \propto L^{-1.4 \pm 0.3}$  and the rates of events brighter than  $M_{V,\text{peak}} = -3(-10)$  is  $\sim 0.5$  ( $0.03$ )  $\text{yr}^{-1}$ . Our ZTF sample shows that their scaling does not extend to higher luminosities. For transients brighter than  $M_{r,\text{peak}} = -11$ , the luminosity function drops at a much steeper rate ( $\frac{dN}{dL} \propto L^{-2.5}$ ), suggesting a broken power-law luminosity function for LRNe. Fig. 12 shows the LRNe rate as a function of peak absolute magnitude derived from our ZTF sample and the Kochanek et al. (2014) scaling. To convert the Galactic rate measurements from Kochanek et al. (2014) to volumetric rates, we follow Howitt et al. (2020) and assume that the LRN rate scales with star-formation. We use a star-formation rate of  $2 M_{\odot} \text{ yr}^{-1}$  for the Milky Way (Licquia & Newman 2015) and an average cosmic star-formation rate of  $0.015 M_{\odot} \text{ yr}^{-1}$  (Madau & Dickinson 2014). The ZTF and Kochanek et al. (2014) rate estimates diverge at high luminosities. The volumetric rate of LRNe with brighter than  $M_r = -11$  ( $-13$ ) derived from the ZTF sample is lower by a factor of  $\approx 5$  ( $100$ ) than that extrapolated from the Kochanek et al. (2014) scaling.

A steeper luminosity function at the brighter end has also been predicted by binary population synthesis models (Howitt et al. 2020). They follow the binary evolution of a population of binary systems with masses drawn from a Kroupa IMF and a binary fraction of unity, and find that 45% of the simulated binaries undergo some form of unstable mass transfer. 38% of these binaries result in stellar mergers while the remaining 62% result in CE ejections. Qualitatively similar results were also obtained by the population synthesis study of Politano

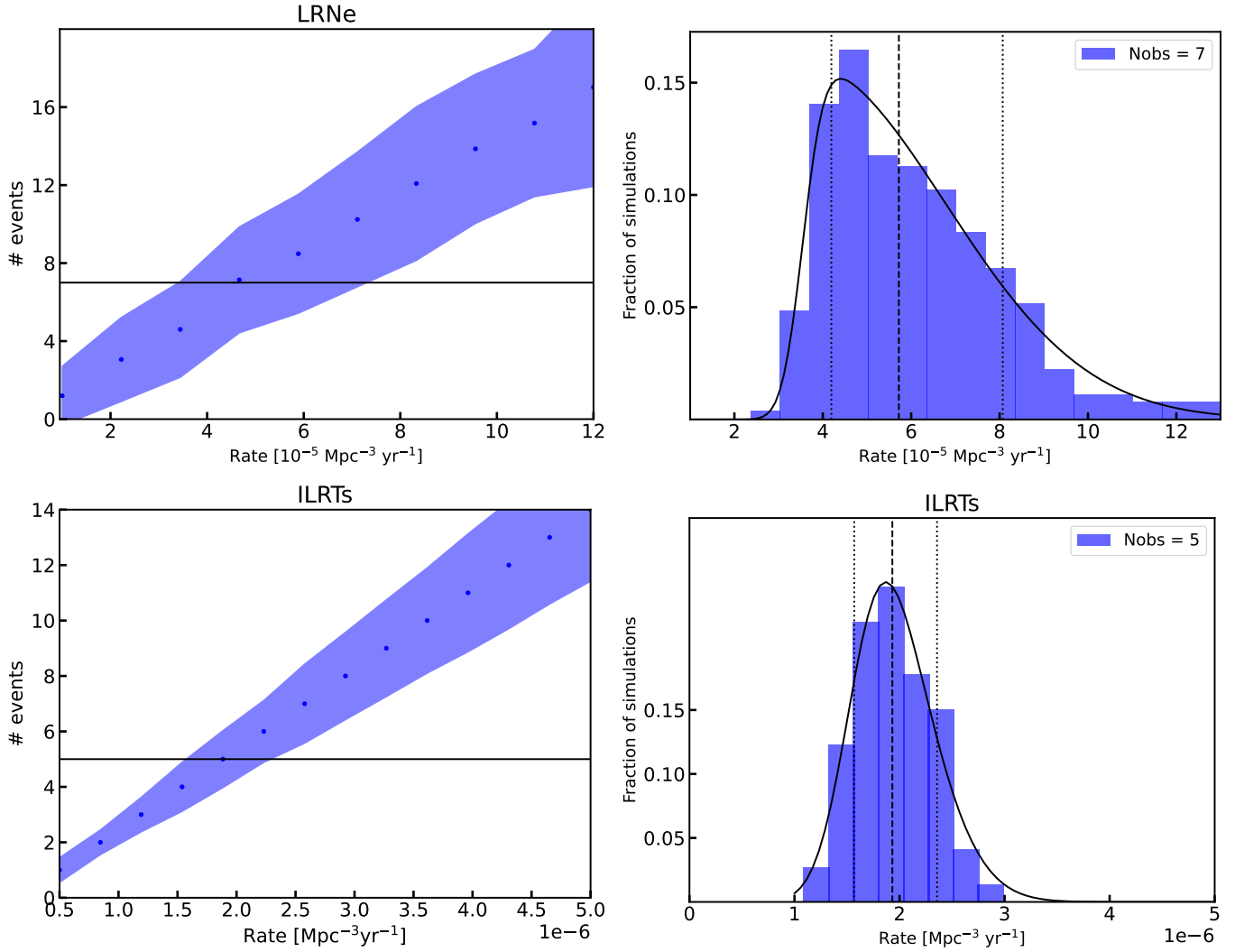


**Figure 11.** *Left:* The number of simulated LRNe (*top*) and ILRTs (*bottom*) that pass our filtering criteria as a function of their volumetric rate. *Right:* The fraction of simulations where the number of simulated transients that pass the filtering criteria LRNe equals the observed number of LRNe (*top*) or ILRTs (*bottom*). The distributions are fit by a skewed gaussian function, indicated as black solid curves. The vertical dashed and dotted lines show the median and 68 percentile confidence limits of the distribution respectively.

et al. (2010), although they focused on the remnants of CEE rather than the associated transients. Howitt et al. (2020) used analytical expressions to approximate lightcurves associated with their simulated mergers and CE ejections, and determined the Galactic rate of LRNe as a function of their peak luminosity. Fig. 12 also shows the volumetric LRN rate from these BPS simulations as a function of peak magnitude. We derive the volumetric rate using the Galactic and average cosmic star-formation rates as described above. As noted by Howitt et al. (2020), the BPS rate agrees with the Kochanek et al. (2014) value for low luminosities, but diverges for  $M_{\text{bol}} \leq -10$ . The step decline in the LRN rate seen in the BPS simulations is consistent with the rates derived from our ZTF sample. However, we note that the

BPS simulations underpredict the rates for LRNe with  $M_r < -13$ . This could be a result of several assumptions about the LRN lightcurves, binary populations or CE physics used in the BPS simulations. Most importantly, Howitt et al. (2020) assumed that the LRN lightcurve is powered solely by hydrogen recombination and used analytical scaling relations from Ivanova et al. (2013b) to estimate a LRN lightcurve. However, as noted in their analysis, this model is unable to reach the luminosities of the highest luminosity LRNe. Similar lightcurve modeling by Matsumoto & Metzger (2022) also shows that hydrogen recombination alone cannot explain the lightcurves of the highest luminosity LRNe. Additionally, hydrogen recombination is believed to power the plateau in LRNe, and not the initial blue peak (which is

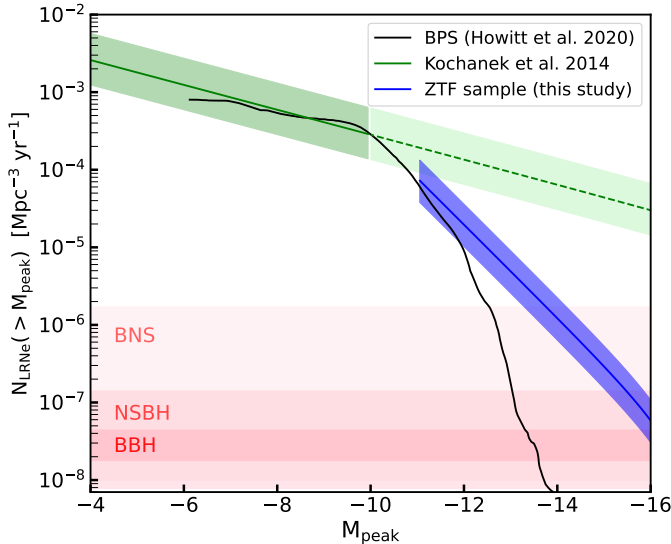


**Figure 12.** The rate of LRNe brighter than a given absolute magnitude as determined from our ZTF sample (blue), the Galactic sample of Kochanek et al. (2014) sample (green) and binary population synthesis models of Howitt et al. (2020) (black line). The Kochanek et al. (2014) sample was restricted to  $-10 \leq M_V \leq -4$ , while the ZTF sample is restricted to  $-16 \leq M_r \leq -11$ . The green dashed-line indicates the Galactic rate extrapolation to brighter luminosities. It is evident that the Galactic scaling overpredicts the observed ZTF rate by several orders of magnitude. The steeper drop of the LRN rate at higher luminosities is also seen in the BPS models. The BPS models underpredict the brightest ( $M_r \leq -13$ ) rate of LRNe, which could be attributed to specific assumptions about CE physics in the models. The pink shaded regions indicate the constraints on the rates of BNS, NSBH and BBH mergers as measured by LIGO (The LIGO Scientific Collaboration et al. 2021a). The rates of the brightest LRNe are consistent with a significant fraction of them being progenitors of these compact merging systems.

used for our and Kochanek et al. 2014 rate calculation). Using the recombination-powered lightcurve model thus underpredicts the LRN rate at the high luminosity end. More accurate models of LRN lightcurves are required to reconcile the predicted rate with the observed rate. Several other parameters about binary populations and CE physics can also contribute to the observed discrepancy. For example, a uniform binary fraction was assumed in the simulations, but the binary fraction increases with stellar mass (Moe & Di Stefano 2017). This would mean the number of massive binaries is higher, which would produce additional LRNe at the bright end.

The broken power-law shape has interesting implications for our sample of LRNe. Observations as well as theoretical models of LRNe predict that the peak luminosities and durations of LRNe directly correlate with their progenitor masses (Kochanek et al. 2014; Blagorod-

nova et al. 2021; Ivanova et al. 2013a; Matsumoto & Metzger 2022; Cai et al. 2022). Using the relation  $L \propto M^{-2.2 \pm 0.3}$  from Cai et al. (2022), our luminosity scaling implies a mass function of  $\frac{dN}{dM} \propto M^{-4.3 \pm 1.1}$ , different from standard IMF models. Kochanek et al. (2014) found that the lower luminosity Galactic LRNe have progenitors consistent with the stellar IMF. An interesting possibility to explain this difference is to postulate that the low luminosity Galactic events are mergers while the more luminous extragalactic events are CE ejections. For a binary system with a given primary mass, the associated LRN is brighter and longer lived if it undergoes complete CE ejection rather than a merger where only a small fraction of the envelope is ejected. From their simulations, Howitt et al. (2020) find that the bright LRNe ( $M_{\text{bol}} \leq -10$ ) result almost exclusively from envelope ejections, while mergers result in lower luminosity transients. The broken power law would then suggest that the luminous CE ejections are much rarer than the less luminous stellar mergers. The range of peak luminosities and durations of the ZTF sample events presented here is consistent with the CE ejections in Howitt et al. (2020). Thus in this picture, most if not all of the events in the ZTF sample analyzed here could be CE ejections. In this case, our derived rate would represent the rate of CE ejections in massive binaries – an important step in the formation of double compact objects (DCOs, Vigna-Gómez et al. 2020). It is interesting to compare our rate to the rate of DCO mergers detected by LIGO. The LIGO Scientific Collaboration et al. (2021b) determined the volumetric rate of binary neutron star (BNS), neutron star-black hole (NSBH) and binary black hole (BBH) mergers as  $10 - 1700 \text{ Gpc}^{-3} \text{ yr}^{-1}$ ,  $7.8 - 140 \text{ Gpc}^{-3} \text{ yr}^{-1}$  and  $17 - 44 \text{ Gpc}^{-3} \text{ yr}^{-1}$  respectively. The shaded pink regions in Fig. 12 indicate these DCO merger rates. The plot shows that the brightest LRNe are consistent with a significant fraction of them being progenitors of DCO mergers.

Finally, we note another possible source of bias that could affect the LRN rate determined here. Pejcha et al. (2017) predict a population of LRNe originating in mergers involving giant primaries that should be completely dust enshrouded, and emit most of their radiation at IR wavelengths. MacLeod et al. (2022) also show that dust formation in pre-merger outflows could obscure the binary system, causing the resulting LRNe to be observable only at IR wavelengths. Some of the IR-only transients, dubbed SPRITES, that were discovered by the *Spitzer Space Telescope* and had no optical counterparts are potential examples of such dust-enshrouded LRNe (Kasliwal et al. 2017). Searches for LRNe at



infrared wavelengths are required to probe this dust-enshrouded population of LRNe. Upcoming NIR time-domain surveys such as the Wide-field Infrared Transient Explorer (WINTER, [Lourie et al. 2020](#)) at the Palomar Observatory and Dynamic REd All-sky Monitoring Survey (DREAMS, [Soon et al. 2020](#)) at the Siding Springs Observatory that are slated to commence operations in the second half of 2022 will help achieve this. Targeted surveys of nearby galaxies with these NIR telescopes will help discover and study IR-only LRNe, and shed light on the complete LRN landscape. Additionally, as all LRNe are brighter and longer lived at NIR wavelengths than the optical, the NIR surveys will also increase the population of optically-selected LRNe similar to those presented in this paper. Of particular importance will be additional discoveries of lower luminosity LRNe ( $-9.5 > M_{r,\text{peak}} > -11$ ) – a luminosity range that has not been probed by our sample as they have much shorter optical lightcurves and can lack the early blue optical peak seen in their brighter counterparts ([Blagorodnova et al. 2021](#)). The upcoming NIR surveys will thus provide an unbiased and more precise measurement of the LRN luminosity function and volumetric rate.

#### 4.2. ILRTs

We derive an ILRT rate of  $R_{<-13.5} \approx 2.6 \times 10^{-6} \text{ Mpc}^{-3} \text{ yr}^{-1}$  for ILRTs that are more luminous than  $M_r = -13.5$  mag. This rate is smaller than the LRN rate by two orders of magnitude, but we note that the luminosity threshold of our ILRT sample is brighter than that of our LRN sample. We cannot constrain the luminosity function of ILRTs with luminosities lower than  $M_r = -13.5$ , as none of our events lie in this luminosity range. In the literature, there are four ILRTs with  $-12 \geq M_r \geq -13.5$ , all discovered long before the start of ZTF ([Cai et al. 2021](#)). Assuming our luminosity function extends to  $M_r \approx -12$ , the total rate of ILRTs is  $R_{<-12} \approx 2 \times 10^{-5} \text{ Mpc}^{-3} \text{ yr}^{-1}$ . Additional discoveries of ILRTs in this low luminosity range are required to map out the lower end of the ILRT luminosity function.

[Cai et al. \(2021\)](#) derived a lower limit on the ILRT rate of  $9 \times 10^{-6} \text{ Mpc}^{-3} \text{ yr}^{-1}$ . They used a sample of 12 ILRTs discovered in the last 12 years within 30 Mpc to estimate the ILRT rate, but their analysis did not include a luminosity function or completeness of the surveys. Additionally, their sample included two events with lower luminosities than our threshold, and their lower limit is consistent with the rough estimate  $R_{<-12}$  above. Comparing to the core-collapse supernova rate of  $\approx 1.01 \times 10^{-4} \text{ Mpc}^{-3} \text{ yr}^{-1}$  ([Perley et al. 2020](#)), we find that the rate of ILRTs ( $R_{<-13.5}$ ) is  $\approx 3_{-1.5}^{+1.5}\%$  of the

CCSN rate. It remains to be seen how much the lower luminosity events contribute to this rate.

Our rate is also lower than the estimate from [Thompson et al. \(2009\)](#) who estimated the ILRT rate is  $\sim 20\%$  of the CCSN rate based on the two ILRTs SN 2008S and NGC 300OT. We note that NGC 300OT is below the luminosity threshold of our sample, and the rough estimate  $R_{<-12}$  is consistent with their result.

Given the possible association of ILRT with ECSNe, it is worth comparing our rate to theoretical predictions. [Poelarends et al. \(2008a\)](#) determine the range of stellar masses expected to undergo ECSN for different mass-loss and convective dredge-up prescriptions, and determine their rate to be  $\approx 4\% - 24\%$  of the CCSN rate. The rate also depends sensitively on the metallicity, e.g. [Poelarends \(2007\)](#) find that for  $Z = 0.02$ , the ECSN rate is  $\approx 3\%$  of the CCSN rate but for  $Z = 10^{-4}$  the rate is  $\approx 25\%$ . On the contrary, [Doherty et al. \(2015\)](#) use a different metallicity dependence on the mass-loss rate and find that the ECSN rate is  $\approx 2 - 5\%$  of the CCSN rate for all metallicities in the range  $Z = [10^{-5}, 0.02]$ . Our measured ILRT rate ( $R_{<-13.5}$ ) is on the lower side, but still consistent with the wide range of theoretical calculations, and it is in line with the interpretation that several ILRTs could be ECSNe.

We note however that we cannot rule out that some of the ILRTs presented here are LBV outbursts. Dusty LBV outbursts can also result in red, low luminosity transients with spectra showing narrow H with Ca II and [Ca II] features, similar to ILRTs ([Andrews et al. 2021](#)). While the transients in our sample do not show any archival activity for the last  $\approx 10$  years, it is possible that they experienced previous outbursts. Nevertheless, the connection of ILRTs to ECSNe is supported by strong evidence related to their dust-enshrouded progenitors with masses between  $8-15 M_{\odot}$  ([Thompson et al. 2009](#); [Botticella et al. 2009](#); [Jencson et al. 2019](#)) and the fact that their remnants faded below their progenitor luminosities ([Adams et al. 2016](#)). Progenitors are not detectable for most of the ILRTs in our sample. As this will also be the case for a large number of ILRTs that will be detected by future large-scale deep surveys such as the Vera Rubin Observatory (VRO, [Ivezić et al. 2019](#)), it is important to identify additional ways of distinguishing ILRTs from LBV outbursts to confirm their nature as ECSNe. Possible ways to achieve this are extensive nebular-phase observations of ILRTs. On the one hand, late-time photometric observations would allow us to detect the presence, and estimate the amount of Ni generated in the explosion (see [Cai et al. 2021](#)). On the other hand, nebular spectroscopic observations would allow us to determine the composition of the ILRT ejecta

where the presence of stronger Ni than Fe lines, weak O, Mg, C, Fe lines and a low [O I]/[Ca II] ratios would be evidence for the ECSN scenario (similar to AT2018zd, Hiramatsu et al. 2021).

#### 4.3. Host galaxies of LRNe and ILRTs

Fig. 13 shows thumbnails of the host galaxies of the ZTF ILRTs presented in this paper. The ZTF ILRTs belong to starforming galaxies, similar to all ILRTs discovered to date (see Cai et al. 2021). As neither ZTF nor the CLU galaxy catalog are biased towards starforming galaxies (Cook et al. 2019), the sample confirms that ILRTs occur in predominantly young environments – consistent with their ECSN or LBV interpretations.

Fig. 14 shows thumbnails of the host galaxies of the ZTF LRNe presented in this paper. All ZTF LRNe also belong to late-type starforming galaxies (see Table 1 for host galaxy morphologies), similar to all LRNe discovered in the last decade (see Pastorello et al. 2019a; Blagorodnova et al. 2021). This confirms that the luminous ( $M_r \leq -11$ ) LRNe occur more commonly in star-forming environments. This is consistent with the expectation that LRNe in this luminosity range have massive ( $\geq 10M_\odot$ ) progenitors (Blagorodnova et al. 2021). Early-type galaxies are expected to have LRNe with lower mass progenitors and hence lower luminosities, making time-domain surveys less sensitive towards detecting them.

Only three LRNe have been discovered in old environments – OGLE2002-BLG-360 in the Galactic bulge (Tylenda et al. 2013), M31RV in the bulge of M31 (Rich et al. 1989) and M85 OT in the S0-type galaxy M85 (Kulkarni et al. 2007). Of these, M85 OT does not follow the LRN peak luminosity-progenitor mass correlation (Kochanek et al. 2014; Blagorodnova et al. 2021). The progenitor mass of M85 OT has been constrained to  $< 7M_\odot$  (Ofek et al. 2008). This is expected to produce a LRN with  $M_{r,\text{peak}} \geq -10$  – much fainter than its actual peak  $M_r \approx -12$ . As it is not a canonical LRN, M85 OT has been suggested to be an ILRT. However, ILRTs have starforming hosts unlike M85 OT. Its progenitor mass is also incompatible with the ECSN or LBV scenario for ILRTs, suggesting that it is not a canonical ILRT either. An intriguing possibility is that M85OT is the merger of a WD with a companion evolved star. Such “CV mergers” are believed to produce transients with observational characteristics similar to LRNe (Metzger et al. 2021). A WD progenitor would be consistent with the old environment of M85OT. As this is not a canonical merger of two stars, we would not expect the transient to follow the correlations observed in other LRNe. The Galactic slow nova CK Vul has been proposed to be a

merger involving a white dwarf progenitor (Eyres et al. 2018; Metzger et al. 2021). M85OT could be an extragalactic member of this class of outbursts. Discoveries of additional LRNe in early-type galaxies will shed further light on the origin of this population.

## 5. SUMMARY AND WAY FORWARD

Despite the discovery of a dozen LRNe and ILRTs in the last decade, their rate remained uncertain. In this paper, we compiled a systematic sample of LRNe and ILRTs using the Census of the Local Universe experiment on the Zwicky Transient Facility to address this issue. We present a sample of eight LRNe and eight ILRTs identified by the CLU experiment. We discuss the properties of these transients, and present new data for the precursor emission in AT2019zhd and line profile evolution in ZTF21aaekekq (AT2021afy). We conduct simulations of the ZTF survey using actual ZTF observation history and correct for the completeness of CLU to derive a rate of  $7.8_{-3.7}^{+6.5} \times 10^{-5} \text{ Mpc}^{-3} \text{ yr}^{-1}$  for LRNe with absolute magnitudes  $M_r$  in the range  $[-11, -16]$ ; and  $2.6_{-1.4}^{+1.8} \times 10^{-6} \text{ Mpc}^{-3} \text{ yr}^{-1}$  for ILRTs with  $M_r < -13.5$ .

The rates of LRNe in this luminosity range are much lower than those extrapolated from Galactic measurements of low luminosity Galactic LRNe by Kochanek et al. (2014). Specifically, we find that the luminosity function of LRNe scales as  $\propto L^{-2.5}$  in the range  $-11 < M_r < -16$ , as opposed to  $L^{-1.4}$  derived by Kochanek et al. (2014) for  $-4 < M_V < -10$ . This steeper decline at higher luminosities is broadly consistent with binary population synthesis models of Howitt et al. (2020), however the BPS models underpredict the rates for  $M_r < -13$  by as much as two orders of magnitude. This discrepancy is likely due to assumptions about the lightcurve models used in the BPS simulation. The rates of the brightest LRNe in our sample are consistent with a significant fraction of them being progenitors of double compact object systems. We note that all LRNe in our sample, and those discovered in the last decade belong to star-forming host galaxies. There have been no analogs of M85 OT that was discovered in a S0-type galaxy.

The ILRT rate corresponds to  $2.6_{-1.4}^{+1.8}\%$  of the local core-collapse SN rate. However, our sample only probes the high luminosity end of the ILRT luminosity function. Assuming our scaling extrapolates to lower luminosities, our measurement is consistent with previously measured constraints on the ILRT rate by Thompson et al. (2009) and Cai et al. (2021). The ILRT rate is also consistent with the wide range of theoretical predictions of rates of electron-capture SNe by Poelarends et al. (2008b) and Doherty et al. (2015). Additional nebular phase obser-

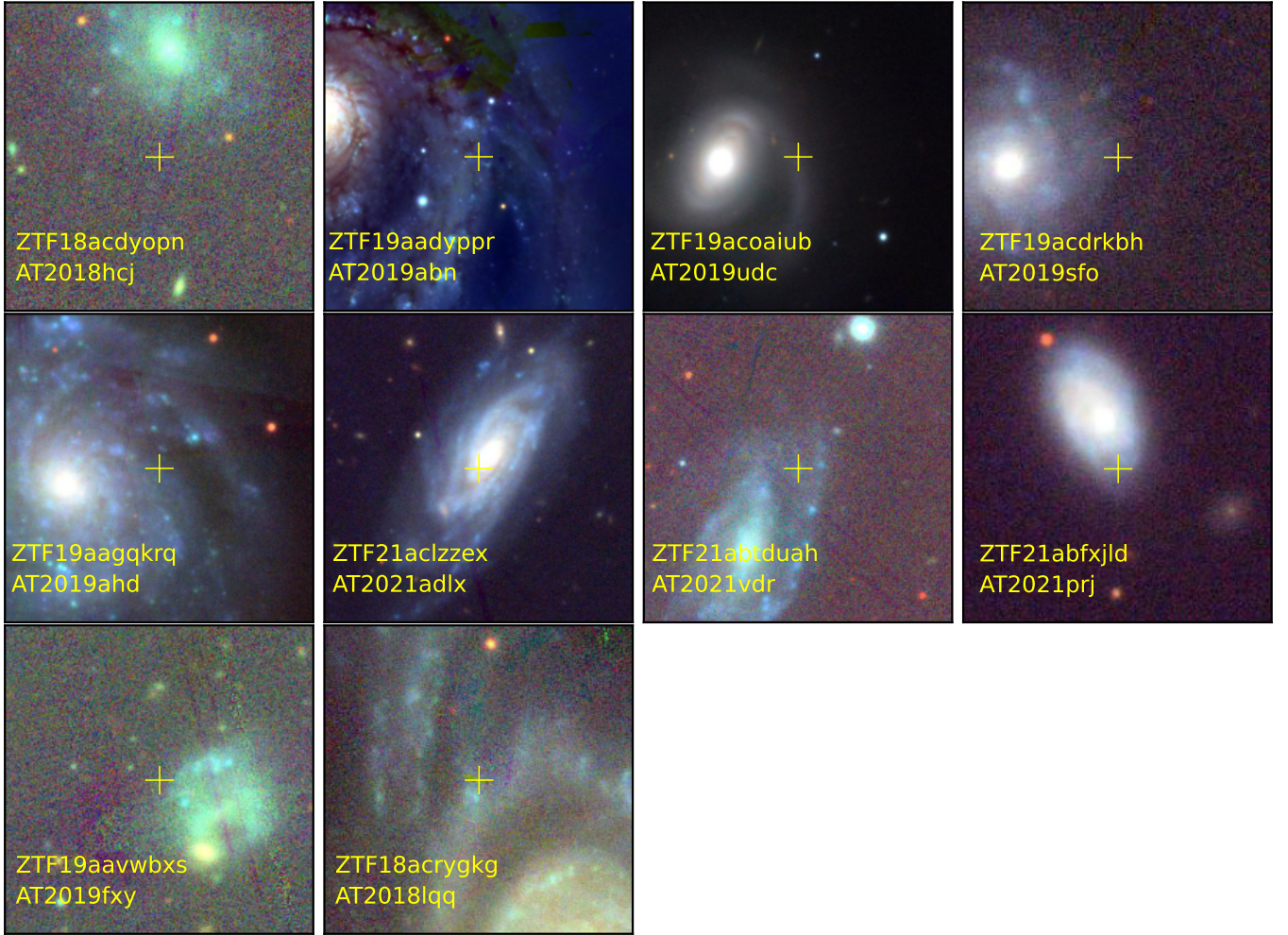


**Figure 13.** Host galaxies of the ILRTs in our sample. The positions of the ILRTs are indicated with a yellow cross, on top of color-coded PS1 images obtained from [here](#). Similar to LRNe, all ILRTs in our sample are located in star-forming galaxies.

vations of ILRTs and observations of their progenitors are required to confidently establish them as electron-capture SNe.

The future holds exciting prospects for studies of LRNe and ILRTs. Upcoming NIR time domain surveys such as WINTER and DREAMS will enable substantial progress in the next few years. These surveys will provide the first unbiased sample of the dusty, red transients and will be instrumental in uncovering hidden populations that could be missed by optical surveys. These results will set the stage for the VRO. Based on our rate estimates, we calculate that VRO will discover between 300 to 1500 LRNe and 200-700 ILRTs (with  $M_{r,\text{peak}} < -13.5$ ) per year (assuming a sensitivity of  $m_r \approx 24.2$  mag). While most of these will be too faint for spectroscopic classifications, these transients can be identified based on their low luminosities, long duration lightcurves and red photometric colors. An experiment similar to the Census of the Local Universe that keeps

track of VRO transients in catalogued galaxies will be instrumental in the study of LRNe and ILRTs.

## 6. ACKNOWLEDGEMENTS

Based on observations obtained with the Samuel Oschin Telescope 48-inch and the 60-inch Telescope at the Palomar Observatory as part of the Zwicky Transient Facility project. ZTF is supported by the National Science Foundation under Grants No. AST-1440341 and AST-2034437 and a collaboration including current partners Caltech, IPAC, the Weizmann Institute of Science, the Oskar Klein Center at Stockholm University, the University of Maryland, Deutsches Elektronen-Synchrotron and Humboldt University, the TANGO Consortium of Taiwan, the University of Wisconsin at Milwaukee, Trinity College Dublin, Lawrence Livermore National Laboratories, IN2P3, University of Warwick, Ruhr University Bochum, Northwestern University and former partners the University of Washington, Los

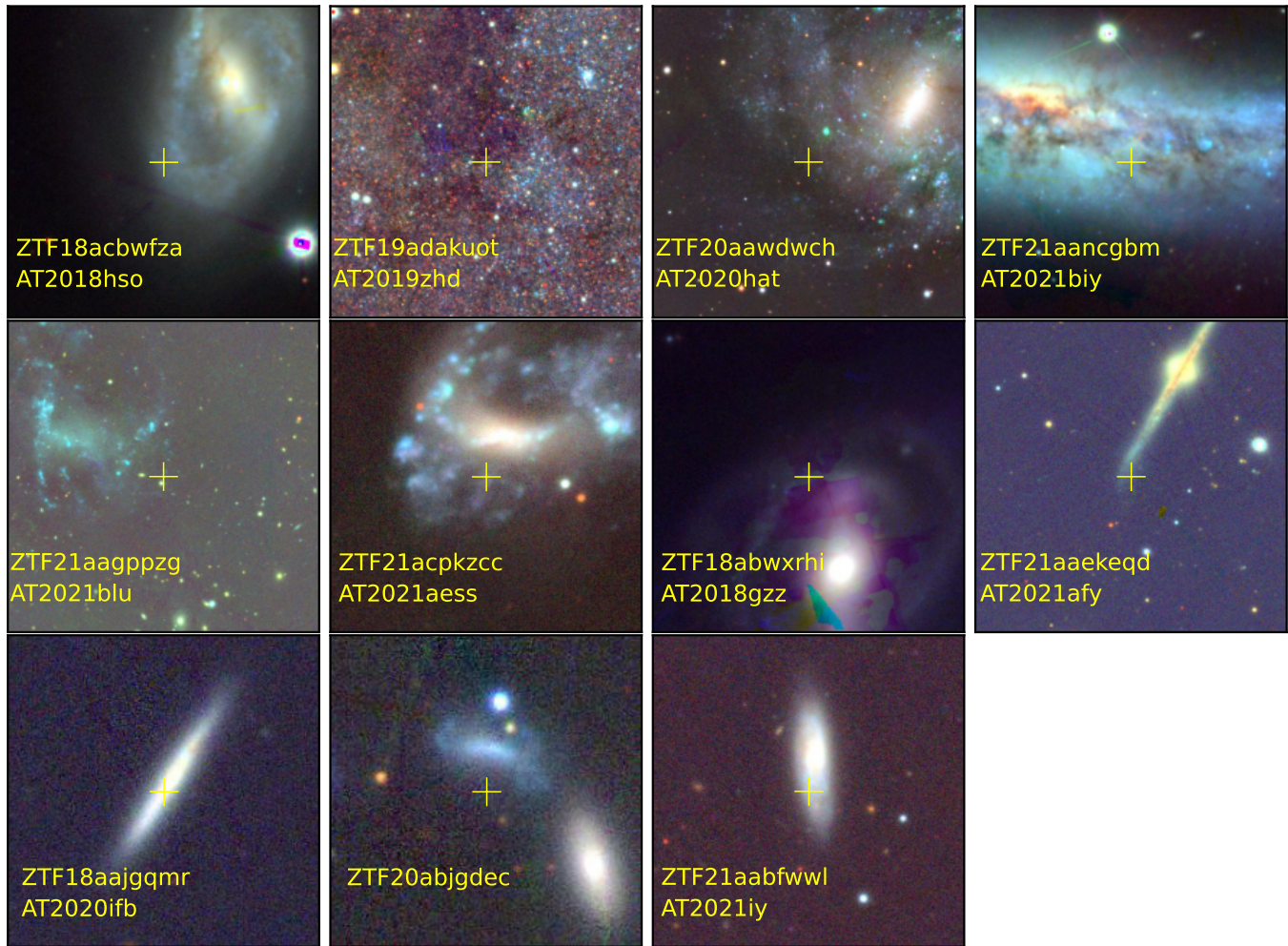


**Figure 14.** Host galaxies of the LRNe in our sample. The positions of the LRNe are indicated with a yellow cross. ZTF 19adakuot is located in M31. All LRNe in our sample (including LRN-bronze events) are located in star-forming galaxies.

Alamos National Laboratories, and Lawrence Berkeley National Laboratories. Operations are conducted by COO, IPAC, and UW. The ZTF forced photometry service was funded under the Heising-Simons Foundation grant 12540303 (PI: Graham). SED Machine is based upon work supported by the National Science Foundation under Grant No. 1106171. This work is also based on observations made with the Nordic Optical Telescope, owned in collaboration by the University of Turku and Aarhus University, and operated jointly by Aarhus University, the University of Turku and the University of Oslo, representing Denmark, Finland and Norway, the University of Iceland and Stockholm University at the Observatorio del Roque de los Muchachos, La Palma, Spain, of the Instituto de Astrofísica de Canarias. SED Machine is based upon work supported by the National Science Foundation under Grant No. 1106171. The Liverpool Telescope is operated on the island of La Palma by Liverpool John Moores University

in the Spanish Observatorio del Roque de los Muchachos of the Instituto de Astrofísica de Canarias with financial support from the UK Science and Technology Facilities Council. This work is part of the research program VENI, with project number 016.192.277, which is partly financed by the Netherlands Organisation for Scientific Research (NWO). A.V.F.’s group acknowledges generous support from the Christopher R. Redlich Fund, the U.C. Berkeley Miller Institute for Basic Research in Science, Sunil Nagaraj, Landon Noll, Sandy Otellini, and many additional donors. A major upgrade of the Kast spectrograph on the Shane 3 m telescope at Lick Observatory, led by Brad Holden, was made possible through generous gifts from the Heising-Simons Foundation, William and Marina Kast, and the University of California Observatories. Research at Lick Observatory is partially supported by a generous gift from Google.

## 7. DATA AVAILABILITY

Lightcurves and spectra of the LRNe, ILRTs and possible LBVs presented in this paper, and template LRN and ILRT lightcurves will be made available online after

publication. The spectra will also be posted to WIS-eREP. The ZTF pointing history logs will be made available upon request to the corresponding author.

## REFERENCES

- Adams, S. M., Kochanek, C. S., Prieto, J. L., et al. 2016, *MNRAS*, 460, 1645
- Andrews, J. E., Jencson, J. E., Van Dyk, S. D., et al. 2021, *ApJ*, 917, 63
- Bellm, E. C., Kulkarni, S. R., Graham, M. J., et al. 2019, *PASP*, 131, 018002
- Bildsten, L., Shen, K. J., Weinberg, N. N., & Nelemans, G. 2007, *ApJ*, 662, L95
- Blagorodnova, N., Neill, J. D., Walters, R., et al. 2018, *PASP*, 130, 035003
- Blagorodnova, N., Karambelkar, V., Adams, S. M., et al. 2020, *MNRAS*, 496, 5503
- Blagorodnova, N., Klencki, J., Pejcha, O., et al. 2021, *A&A*, 653, A134
- Botticella, M. T., Pastorello, A., Smartt, S. J., et al. 2009, *MNRAS*, 398, 1041
- Bramall, D. G., Sharples, R., Tyas, L., et al. 2010, in *Society of Photo-Optical Instrumentation Engineers (SPIE) Conference Series*, Vol. 7735, *Ground-based and Airborne Instrumentation for Astronomy III*, ed. I. S. McLean, S. K. Ramsay, & H. Takami, 77354F
- Cai, Y. Z., Pastorello, A., Fraser, M., et al. 2019, *A&A*, 632, L6
- . 2021, *A&A*, 654, A157
- . 2022, arXiv e-prints, arXiv:2207.00734
- Cook, D. O., Kasliwal, M. M., Van Sistine, A., et al. 2019, *ApJ*, 880, 7
- Davis, K., Jones, D., Bustamante-Rosell, M. J., Siebert, M., & Foley, R. 2021, *Transient Name Server Classification Report*, 2021-3967, 1
- De, K., Kasliwal, M. M., Tzanidakis, A., et al. 2020, *ApJ*, 905, 58
- Dekany, R., Smith, R. M., Riddle, R., et al. 2020, *PASP*, 132, 038001
- Doherty, C. L., Gil-Pons, P., Siess, L., Lattanzio, J. C., & Lau, H. H. B. 2015, *MNRAS*, 446, 2599
- Eyres, S. P. S., Evans, A., Zijlstra, A., et al. 2018, *MNRAS*, 481, 4931
- Feindt, U., Nordin, J., Rigault, M., et al. 2019, *Journal of Cosmology and Astroparticle Physics*, 2019, 005
- Fremling, C., Miller, A. A., Sharma, Y., et al. 2020, *ApJ*, 895, 32
- Graham, M. J., Kulkarni, S. R., Bellm, E. C., et al. 2019, *PASP*, 131, 078001
- Herter, T. L., Henderson, C. P., Wilson, J. C., et al. 2008, in *Society of Photo-Optical Instrumentation Engineers (SPIE) Conference Series*, Vol. 7014, *Proc. SPIE*, 70140X
- Hinkle, J. 2021, *Transient Name Server Classification Report*, 2021-64, 1
- Hiramatsu, D., Howell, D. A., Van Dyk, S. D., et al. 2021, *Nature Astronomy*, 5, 903
- Howitt, G., Stevenson, S., Vigna-Gómez, A., et al. 2020, *MNRAS*, 492, 3229
- Humphreys, R. M., Bond, H. E., Bedin, L. R., et al. 2011, *ApJ*, 743, 118
- Humphreys, R. M., Davidson, K., & Smith, N. 1999, *PASP*, 111, 1124
- Ivanova, N., Justham, S., Avendano Nandez, J. L., & Lombardi, J. C. 2013a, *Science*, 339, 433
- Ivanova, N., Justham, S., Chen, X., et al. 2013b, *A&A Rev.*, 21, 59
- Ivezić, Ž., Kahn, S. M., Tyson, J. A., et al. 2019, *ApJ*, 873, 111
- Jencson, J. E., Adams, S. M., Bond, H. E., et al. 2019, *ApJ*, 880, L20
- Kamiński, T., Mason, E., Tylanda, R., & Schmidt, M. R. 2015, *A&A*, 580, A34
- Kamiński, T., & Tylanda, R. 2011, *A&A*, 527, A75
- Karambelkar, V. R., Kasliwal, M. M., Maguire, K., et al. 2021, *ApJ*, 921, L6
- Kasliwal, M. M., Kulkarni, S. R., Arcavi, I., et al. 2011, *ApJ*, 730, 134
- Kasliwal, M. M., Bally, J., Masci, F., et al. 2017, *ApJ*, 839, 88
- Kim, Y. L., Rigault, M., Neill, J. D., et al. 2022, *PASP*, 134, 024505
- Kochanek, C. S., Adams, S. M., & Belczynski, K. 2014, *MNRAS*, 443, 1319
- Kulkarni, S. R., Ofek, E. O., Rau, A., et al. 2007, *Nature*, 447, 458
- Law, N. M., Kulkarni, S. R., Dekany, R. G., et al. 2009, *PASP*, 121, 1395
- Licquia, T. C., & Newman, J. A. 2015, *ApJ*, 806, 96
- Lourie, N. P., Baker, J. W., Burruss, R. S., et al. 2020, in *Society of Photo-Optical Instrumentation Engineers (SPIE) Conference Series*, Vol. 11447, *Society of Photo-Optical Instrumentation Engineers (SPIE) Conference Series*, 114479K

- MacLeod, M., De, K., & Loeb, A. 2022, arXiv e-prints, arXiv:2205.07929
- MacLeod, M., Macias, P., Ramirez-Ruiz, E., et al. 2017, *ApJ*, 835, 282
- Madau, P., & Dickinson, M. 2014, *ARA&A*, 52, 415
- Masci, F. J., Laher, R. R., Rusholme, B., et al. 2019, *PASP*, 131, 018003
- Matsumoto, T., & Metzger, B. D. 2022, arXiv e-prints, arXiv:2202.10478
- Metzger, B. D., Zenati, Y., Chomiuk, L., Shen, K. J., & Strader, J. 2021, *ApJ*, 923, 100
- Moe, M., & Di Stefano, R. 2017, *ApJS*, 230, 15
- Munari, U., Henden, A., Kiyota, S., et al. 2002, *A&A*, 389, L51
- Ofek, E. O., Kulkarni, S. R., Rau, A., et al. 2008, *ApJ*, 674, 447
- Oke, J. B., & Gunn, J. E. 1982, *PASP*, 94, 586
- Oke, J. B., Cohen, J. G., Carr, M., et al. 1995, *PASP*, 107, 375
- Pastorello, A., & Fraser, M. 2019, *Nature Astronomy*, 3, 676
- Pastorello, A., Mason, E., Taubenberger, S., et al. 2019a, *A&A*, 630, A75
- Pastorello, A., Chen, T.-W., Cai, Y.-Z., et al. 2019b, *A&A*, 625, L8
- Pastorello, A., Fraser, M., Valerin, G., et al. 2021a, *A&A*, 646, A119
- Pastorello, A., Valerin, G., Fraser, M., et al. 2021b, *A&A*, 647, A93
- . 2022, arXiv e-prints, arXiv:2208.02782
- Pejcha, O., Metzger, B. D., Tyles, J. G., & Tomida, K. 2017, *ApJ*, 850, 59
- Perley, D. A., Fremling, C., Sollerman, J., et al. 2020, *ApJ*, 904, 35
- Poelarends, A. J. T. 2007, PhD thesis, University of Utrecht, Netherlands
- Poelarends, A. J. T., Herwig, F., Langer, N., & Heger, A. 2008a, *ApJ*, 675, 614
- . 2008b, *ApJ*, 675, 614
- Politano, M., van der Sluys, M., Taam, R. E., & Willems, B. 2010, *ApJ*, 720, 1752
- Poznanski, D., Prochaska, J. X., & Bloom, J. S. 2012, *MNRAS*, 426, 1465
- Prieto, J. L., Kistler, M. D., Thompson, T. A., et al. 2008, *ApJ*, 681, L9
- Rau, A., Kulkarni, S. R., Law, N. M., et al. 2009, *PASP*, 121, 1334
- Reguitti, A., Pumo, M. L., Mazzali, P. A., et al. 2021, *MNRAS*, 501, 1059
- Rich, R. M., Mould, J., Picard, A., Frogel, J. A., & Davies, R. 1989, *ApJ*, 341, L51
- Rigault, M., Neill, J. D., Blagorodnova, N., et al. 2019, *A&A*, 627, A115
- Schlafly, E. F., & Finkbeiner, D. P. 2011, *ApJ*, 737, 103
- Schlafly, E. F., Finkbeiner, D. P., Jurić, M., et al. 2012, *ApJ*, 756, 158
- Smith, K. W., Smartt, S. J., Young, D. R., et al. 2020, *PASP*, 132, 085002
- Smith, K. W., Shingles, L., Srivastav, S., et al. 2021a, *Transient Name Server AstroNote*, 33, 1
- Smith, K. W., Srivastav, S., McBrien, O., et al. 2021b, *Transient Name Server AstroNote*, 43, 1
- Smith, N., Andrews, J. E., Mauerhan, J. C., et al. 2016, *MNRAS*, 455, 3546
- Smith, N., Li, W., Silverman, J. M., Ganeshalingam, M., & Filippenko, A. V. 2011, *MNRAS*, 415, 773
- Smith, N., Ganeshalingam, M., Chornock, R., et al. 2009, *ApJ*, 697, L49
- Soon, J., Adams, D., De, K., et al. 2020, in *Advances in Optical Astronomical Instrumentation*, 5
- The LIGO Scientific Collaboration, the Virgo Collaboration, the KAGRA Collaboration, et al. 2021a, arXiv e-prints, arXiv:2111.03606
- . 2021b, arXiv e-prints, arXiv:2111.03634
- Thompson, T. A., Prieto, J. L., Stanek, K. Z., et al. 2009, *ApJ*, 705, 1364
- Tonry, J. L., Denneau, L., Heinze, A. N., et al. 2018, *PASP*, 130, 064505
- Turatto, M., Benetti, S., & Cappellaro, E. 2003, in *From Twilight to Highlight: The Physics of Supernovae*, ed. W. Hillebrandt & B. Leibundgut, 200
- Tylenda, R. 2005, *A&A*, 436, 1009
- Tylenda, R., Hajduk, M., Kamiński, T., et al. 2011, *A&A*, 528, A114
- Tylenda, R., Kamiński, T., Udalski, A., et al. 2013, *A&A*, 555, A16
- Uno, K., Kawabata, M., & Taguchi, K. 2021, *Transient Name Server Classification Report*, 2021-393, 1
- van der Walt, S. J., Crellin-Quick, A., & Bloom, J. S. 2019, *Journal of Open Source Software*, 4, doi:10.21105/joss.01247
- Vigna-Gómez, A., MacLeod, M., Neijssel, C. J., et al. 2020, *Publications of the Astronomical Society of Australia*, 37, e038
- Wilson, J. C., Henderson, C. P., Herter, T. L., et al. 2004, in *Society of Photo-Optical Instrumentation Engineers (SPIE) Conference Series*, Vol. 5492, *Ground-based Instrumentation for Astronomy*, ed. A. F. M. Moorwood & M. Iye, 1295–1305
- Yang, S., Sollerman, J., Strotjohann, N. L., et al. 2021, *A&A*, 655, A90

## APPENDIX

## A. PROPERTIES OF SOURCES CLASSIFIED AS POSSIBLE LBV OUTBURSTS

The lightcurves of the six sources we classify as potential LBV outbursts are shown in Fig. 15 and their spectra are shown in Fig. 16. We discuss the individual objects below.

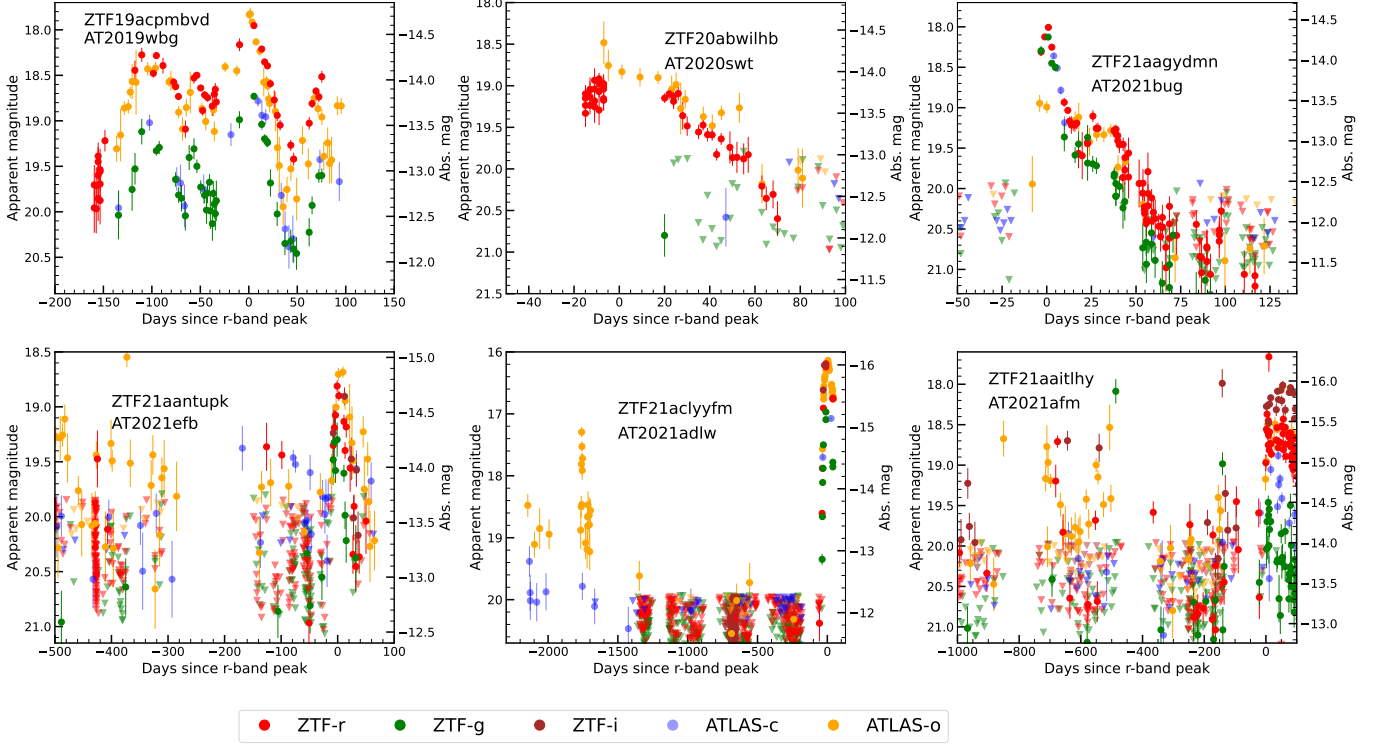
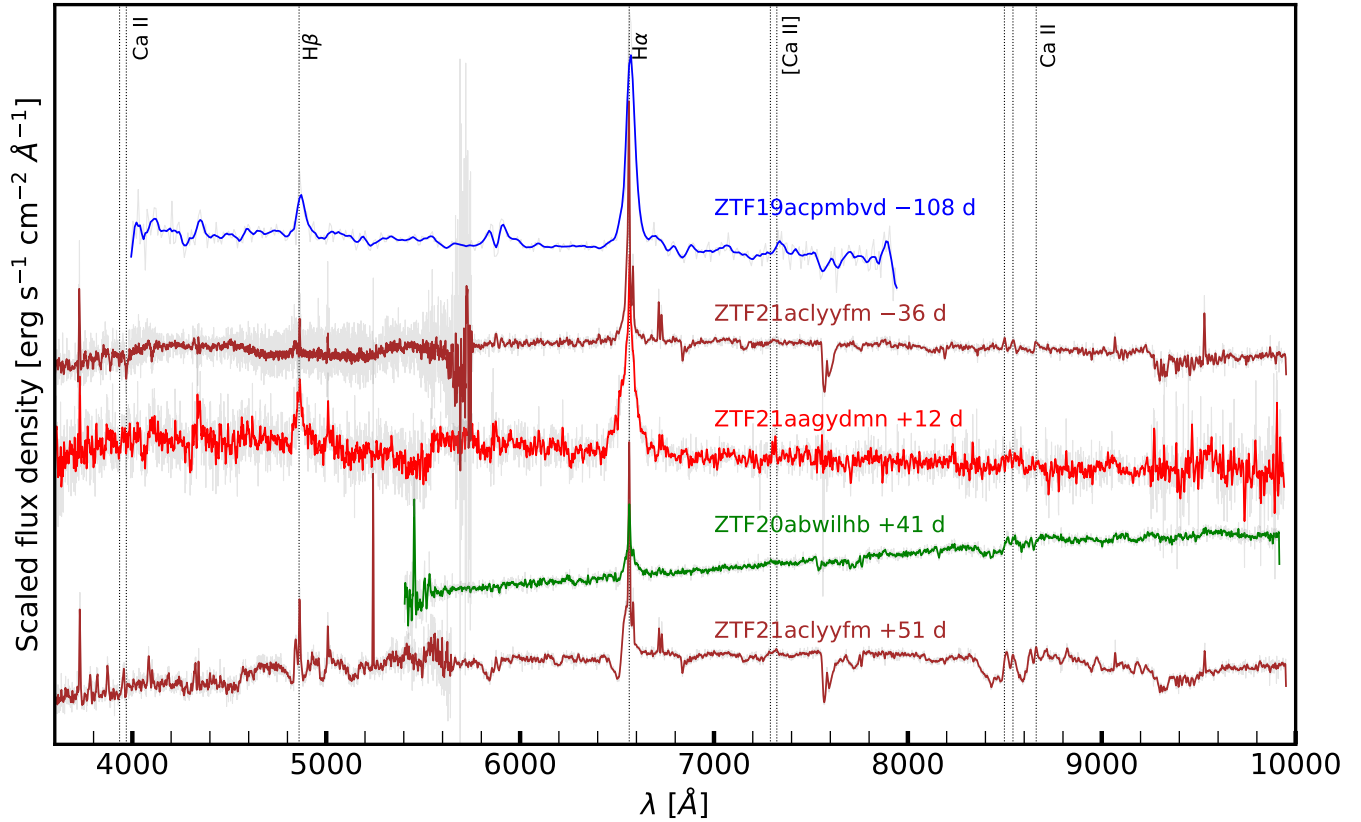


Figure 15. Lightcurves of transients that are possible LBV outbursts

- **ZTF 19acpmbvd (AT 2019wbg)** is located in the galaxy NGC 4045, and shows a bumpy, red lightcurve with at least three peaks. The transient was detected in 2016 in iPTF data with  $m_g \approx 22$  mag. It was redetected in ZTF in 2022 at  $m_r \approx 19.5$  mag. A spectrum taken during this outburst shows  $H\alpha$  with  $v_{\text{FWHM}} \approx 1700 \text{ km s}^{-1}$ .
- **ZTF 20abwilhb (AT 2020swt)** is located in the galaxy UGC 03820. The lightcurve does not show multiple peaks, but shows signs of a  $\approx 40$  day long plateau, after which the transient declines. The optical spectrum shows  $H\alpha$  with  $v_{\text{FWHM}} \approx 3300 \text{ km s}^{-1}$ , suggesting that this transient could be an LBV outburst or a low luminosity Type II SN.
- **ZTF 21aagydmn (AT 2021bug)** is located in the galaxy NGC 4533 and shows an unusual lightcurve that peaks at  $M_r \approx -14.4$  and declines quickly. Once off the first decline, the lightcurve plateaus for  $\approx 10$  days, and then continues to decline. The spectrum shows  $H\alpha$  with  $v_{\text{FWHM}} \approx 2600 \text{ km s}^{-1}$ , however the lightcurve does not show a long-duration plateau as seen in low luminosity Type II SNe. The true nature of this source is unclear, but an outburst in a massive star is a possibility.
- **ZTF 21aantupk (AT 2021efb)** is located at the nucleus of the galaxy CGC 003-005. The lightcurve shows erratic activity in the ATLAS and the ZTF data prior for several hundred days prior to the main explosion in 2021. We suggest that this source is either an LBV outburst or AGN activity.
- **ZTF 21aclyyfm (AT 2021adlw)** is located in the galaxy NGC 3813, and reached a peak absolute magnitude of  $M_r \approx -16$  in the 2021 outburst. Archival ATLAS data shows that it underwent a similar outburst ( $M_o \approx -15$ )



**Figure 16.** Optical spectra of transients that are possible LBV outbursts

$\approx 1800$  days prior to this outburst. An optical spectrum taken at an early phase during the 2021 outburst shows narrow  $H\alpha$  with  $v_{\text{FWHM}} \approx 1000 \text{ km s}^{-1}$ , however late time spectra show ejecta with much larger velocities. This source is likely an LBV outburst or a “weak” Type II $n$  supernova.

- **ZTF 21aaitlhy (AT 2021afm)** is located close to the center of the galaxy NGC 5657. It shows several detections in ATLAS and ZTF data in the  $\approx 1000$  days leading up to the 2021 explosion. We also detect the transient in the  $g$ -band in PTF data taken during July 2011 and April 2016 at  $m_g \approx 20$  mag. Owing to the extensive archival activity, we categorize this source as a possible LBV outburst.